

Methane, carbon dioxide and nitrous oxide emissions from two clear-water and two turbid-water urban ponds in Brussels (Belgium)

Thomas Bauduin ^{1,2}, Nathalie Gypens ¹, Alberto V. Borges ²

¹Ecology of Aquatic Systems, Université Libre de Bruxelles, Belgium

²Chemical Oceanography Unit, University of Liège, Belgium

Correspondence to: Thomas Bauduin (thomas.bauduin@ulb.be)

Abstract. Shallow ponds can ~~exist-occur~~ either in a clear-water state dominated by macrophytes or a turbid-water state dominated by phytoplankton, but it is unclear if ~~and how~~ these two states affect ~~differently~~ the emission to the atmosphere of greenhouse gases (GHGs) such as carbon dioxide (CO₂), methane (CH₄) and nitrous oxide (N₂O) ~~emissions to the atmosphere~~. We measured on 46 occasions over 2.5 years (between June 2021 and December 2023) the dissolved concentration of CO₂, CH₄, and N₂O from which the diffusive air-water fluxes were computed, in four urban ponds in the city of Brussels (Belgium): ~~two clear-water urban ponds (Silex and Tenreuken) dominated by macrophytes~~ macrophyte-dominated ponds (Silex and Tenreuken), and two turbid-water ~~urban ponds (Leybeek and Pêcherie) dominated by phytoplankton~~ phytoplankton-dominated ponds (Leybeek and Pêcherie), ~~in the city of Brussels (Belgium), were sampled 46 times between June 2021 and December 2023 to measure the partial pressure of CO₂ (pCO₂), dissolved CH₄ concentration, N₂O saturation level (%N₂O), and ancillary variables~~. CH₄ ebullitive fluxes were measured with bubble traps in the four ponds during deployments in spring, summer, and fall, ~~also measured in the four ponds during 8 deployments, totalling 48 days of cumulated measurements~~. To characterize methanogenic pathways (acetoclastic or hydrogenotrophic) and quantify water column methane oxidation (MOX) we measured ~~the~~ ¹³C/¹²C ratio of CH₄ (δ¹³C-CH₄) from gas trapped in the bubble traps, from bubbles deliberately released by the perturbation of the sediments, and in dissolved CH₄ in the water column. Measured ancillary variables include water temperature, oxygen saturation level (%O₂), concentrations of chlorophyll-*a* (Chl-*a*), total suspended matter (TSM), soluble reactive phosphorus (SRP), nitrite (NO₂⁻), nitrate (NO₃⁻) and ammonium (NH₄⁺). ~~was measured in bubbles from the sediment and in water to decipher the pathway of sedimentary methanogenesis (acetoclastic or hydrogenotrophic) and quantify methane oxidation (MOX) in the water column. The pCO₂ and CH₄ values in the sampled urban ponds correlated with precipitation and water temperature, respectively. The %N₂O values did not correlate with dissolved inorganic nitrogen (DIN) nor other variables for the individual ponds, but a positive relation to DIN emerged from the combined data set for the four ponds. The sampled turbid-water and clear-water ponds did not show differ significantly differences~~ in terms of diffusive emissions of CO₂ and N₂O. Clear-water (macrophyte-dominated) ponds exhibited higher values of annual ebullitive CH₄ fluxes compared to turbid-water (phytoplankton-dominated) ponds, most probably in relation to the delivery to sediments of organic matter from macrophytes. At seasonal scale, CH₄ ~~emissions fluxes between the surface of the ponds and the atmosphere~~ exhibited a temperature dependence in all four ponds, with ebullitive CH₄ fluxes having a stronger dependence to temperature than diffusive CH₄ fluxes. The temperature sensitivity of ebullitive CH₄ fluxes ~~was different among the four ponds and~~ decreased with increasing water depth. In summer, the δ¹³C-CH₄ values of sediment bubbles indicated that the hydrogenotrophic methanogenesis pathway seemed to dominate in clear-water ponds and acetoclastic methanogenesis pathway seemed to dominate in turbid-water ponds. The δ¹³C-CH₄ values of bubbles traps suggested a seasonal shift from the acetoclastic methanogenesis pathway in spring-summer to the hydrogenotrophic methanogenesis pathway in fall. ~~During summer 2023, hydrogenotrophic methanogenesis pathway seemed to dominate in clear water ponds and acetoclastic methanogenesis pathway seemed to dominate in turbid water~~

ponds, as indicated by the $\delta^{13}\text{C}-\text{CH}_4$ values of bubbles sampled by physically perturbing sediments. The $\delta^{13}\text{C}-\text{CH}_4$ values of bubbles sampled during bubble trap deployments in 2021–2023 indicated a seasonal shift to hydrogenotrophic methanogenesis pathway in fall compared to spring and summer, when acetoclastic methanogenesis pathway seemed to dominate. The $\delta^{13}\text{C}-\text{CH}_4$ of dissolved CH_4 indicated higher rates of MOX in turbid-water ponds compared to clear-water ponds, with an overall positive correlation with total suspended matter (TSM) and Chlorophyll *a* (Chl-*a*) concentrations. The presence of suspended particles putatively enhanced MOX by reducing light inhibition of MOX and/or by serving as substrate in the water column for fixed methanotrophic bacteria in the water column. Total CH_4 emissions (diffusive+ebullitive) in CO_2 equivalents either equalized or exceeded those of CO_2 in most ponds, while N_2O emissions were negligible compared to the other two greenhouse gases (GHGs). Total annual GHG emissions in CO_2 equivalents from all four ponds increased from 2022 to 2023 due to higher CO_2 diffusive fluxes, likely driven by higher annual precipitation in 2023 compared to 2022, possibly in response to the intense El Niño event of 2023.

1. Introduction

Greenhouse gas (GHG) emissions from inland water (rivers, lakes, and reservoirs) Emissions to the atmosphere from inland waters (rivers, lakes, and reservoirs) of greenhouse gases (GHGs) such as carbon dioxide (CO_2), methane (CH_4) and nitrous oxide (N_2O) are quantitatively important for global budgets (Lauerwald et al., 2023). GHG emissions from lakes are lower than from rivers for CO_2 (Raymond et al., 2013) and N_2O (Lauerwald et al., 2019; Maavara et al., 2019). However, emissions of CH_4 from lakes (Rosentreter et al., 2021; Johnson et al., 2022) are significant compared to rivers (Stanley et al., 2016; Rocher-Ros et al., 2023). Emissions of CO_2 and CH_4 from lakes to the atmosphere represent 1.25 to 2.30 Pg CO_2 equivalents ($\text{CO}_2\text{-eq}$) annually with a significant proportion from CH_4 emissions, and represent nearly 20% of global CO_2 emissions from fossil fuels (Delsontro et al., 2018). The contribution of CO_2 and CH_4 emissions from small lentic water bodies (small lakes and ponds) could be disproportionately high compared to large systems (Holgerson and Raymond, 2016) as shallow small lakes and ponds are the most abundant of all lake-water body types in number (Verpoorter et al., 2014; Cael et al., 2017), and flux intensities (per m^2) are usually higher in smaller water bodies. The emissions of GHGs from artificial ponds-water bodies such as (agricultural reservoirs, urban ponds, and storm-water retention basins,...) could be higher than those from natural systems (Martinez-Cruz et al., 2017; Grinham et al., 2018; Herrero Ortega et al., 2019; Gorsky et al., 2019; Ollivier et al., 2019; Peacock et al., 2019, 2021; Webb et al., 2019; Bauduin et al., 2024). This-These higher emissions seems to result from higher external inputs of anthropogenic carbon and nitrogen in artificial systems such as rainfall runoff that brings organic matter and dissolved inorganic nitrogen (DIN), but might also reflect other differences compared to natural systems such as in hydrology (Clifford and Heffernan, 2018). Among artificial systems, urban ponds are the subject of a growing body of literature have been seldom investigated for GHG emissions (Singh et al., 2000; Natchimuthu et al., 2014; van Bergen et al., 2019; Audet et al., 2020; Peacock et al., 2021; Goeckner et al., 2022; Ray and Holgerson, 2023; Bauduin et al., 2024). Urban areas can have many-numerous small artificial water bodies mostly associated to green spaces such as public parks, and their number is increasing due to rapid urbanisation worldwide (Brans et al., 2018; Audet et al., 2020; Gorsky et al., 2024; Rabaey et al., 2024). Urban ponds are generally small, shallow, and usually their catchment consists in majority of surrounded-by impervious surfaces with a smaller contribution from soils (Davidson et al., 2015; Peacock et al., 2021). Runoff results in high inputs of organic matter and dissolved inorganic nitrogen (DIN) that sustain production and emission of CO_2 , CH_4 , and N_2O to the atmosphere.

In shallow ponds and lakes, including urban ponds, submerged-aquatic primary production is either dominated by submerged macrophytes or by phytoplankton, corresponding to two alternate states (Scheffer et al., 1993). These two alternative states

correspond to clear waters (macrophyte-dominated) or turbid waters (phytoplankton-dominated), during the productive periods of the year (spring and summer in mid-latitudes). Submerged macrophytes and phytoplankton regulate CO₂ dynamic directly through photosynthesis that can be more or less balanced by community respiration in the water column. However, it is not clear whether the presence of macrophytes increases or decreases the CO₂ emissions from ponds and lakes. Some studies have shown a decrease of CO₂ emissions with increasing macrophyte density (Kosten et al., 2010; Ojala et al., 2011; Davidson et al., 2015), but other studies showed the opposite pattern (Theus et al., 2023). In phytoplankton-dominated lakes, CO₂ concentrations depend in part on the development stage of the phytoplankton, with the growth and peak phases generally coinciding with lower CO₂ concentrations due to intense photosynthesis (Grasset et al., 2020; Vachon et al., 2020). CH₄ emissions have been reported to increase with the concentration of chlorophyll-*a* (Chl-*a*) in phytoplankton-dominated lakes (DelSontro et al., 2018; Borges et al., 2022). The presence of macrophytes strongly affects CH₄ cycling in freshwaters (Bastviken et al., 2023) and vegetated littoral zones of lakes exhibit higher CH₄ emissions than non-vegetated zones (Desrosiers et al., 2022; Theus et al., 2023). Macrophytes influence ~~sediment and~~ organic matter decomposition processes in sediments depending on the quality and quantity of plant matter they release into their environment (Reitsema et al., 2018; Grasset et al., 2019; Harpenslager et al., 2022; Theus et al., 2023). Yet, few studies have consistently compared CH₄ emissions in clear-water and turbid-water ponds (Hilt et al., 2017). A study in Argentina reported higher dissolved CH₄ concentrations in ~~natural~~ clear-water ponds with submerged macrophytes compared to turbid-water ~~phytoplankton dominated~~ phytoplankton-dominated ponds, but no differences in measured CH₄ emissions (Baliña et al., 2023). The production of N₂O predominantly occurs through microbial nitrification and denitrification that depend on DIN and O₂ levels (Codispoti and Christensen, 1985; Mengis et al., 1997). Competition for DIN between primary producers and N₂O-producing microorganisms can impact N₂O production. Additionally, the transfer of labile phytoplankton organic matter to sediments fuels benthic denitrification. Combined, these two processes could explain that some lakes can act as sinks of N₂O under elevated Chl-*a* concentrations (Webb et al., 2019; Borges et al., 2022). The presence of macrophytes also strongly influences nitrogen cycling in sediments of lakes and ponds (Barko et al., 1991; Choudhury et al., 2018; Deng et al., 2020; Dan et al., 2021) and should in theory also affect N₂O emissions, although seldom investigated, and available studies provide contradictory conclusions. ~~Ni et al. (2022) showed that~~ N₂O emissions ~~has been showed to~~ followed diurnal cycles, ~~peaking in the middle of the day when~~ of O₂ concentrations ~~were maximal~~ in areas dominated by submerged macrophytes in Lake Wuliangsuhai (China) (Ni et al., 2022) and ~~Yang et al. (2012) showed that N₂O emissions followed~~ the seasonal cycle of aboveground biomass of emerged macrophytes (*Phragmites*) in Baiyangdian Lake (China) (Yang et al., 2012). On the contrary, some studies showed there were no significant differences of ~~denitrification and~~ N₂O production in sediments of macrophyte-rich (n=10) and macrophyte-free (n=12) lakes in subtropical China (Liu et al., 2018). ~~There have been a very limited number of studies investigating systematically how emissions differ between ponds dominated by phytoplankton and those dominated by macrophytes (Harpenslager et al., 2022; Baliña et al., 2023), and none investigating simultaneously CO₂, CH₄, and N₂O emissions including both diffusive and ebullitive components.~~

The emissions from aquatic systems of CO₂ and N₂O are exclusively through diffusion across the air-water interface (diffusive flux), while CH₄ can be additionally emitted as bubbles released from sediments to the atmosphere (ebullitive flux). ~~At annual scale, The~~ ebullitive CH₄ flux usually represents more than half of total (diffusive+ebullitive) CH₄ emissions from shallow lakes (Wik et al., 2013; Deemer and Holgerson, 2021), ~~although the relative contribution of ebullitive and diffusive CH₄ emissions is highly variable seasonally (e.g. Wik et al., 2023; Ray and Holgerson, 2023).~~ Ebullitive CH₄ fluxes are particularly high in the littoral zone of lakes at depths <5 m (Wik et al., 2013; DelSontro et al., 2016; Borges et al., 2022) and strongly increase in response to temperature (DelSontro et al., 2016; Aben et al., 2017), as well as organic matter availability (DelSontro et al., 2016; 2018). Ebullitive CH₄ fluxes tend to be higher in small and shallow water bodies

119 (Deemer and Holgerson, 2021) but are notoriously variable in time and space, and are difficult to estimate reliably
 120 (DelSontro et al., 2011).

121 The two primary metabolic pathways for CH₄ production in sediments by methanogenic archaea are the fermentation of
 122 acetate (acetoclastic pathway) and the reduction of carbon dioxide by H₂ (hydrogenotrophic pathway) (Whiticar et al., 1986;
 123 Conrad, 1989). CH₄ produced by these two pathways exhibits distinct ¹³C/¹²C ratios (δ¹³C-CH₄) (Whiticar et al., 1986) and
 124 can be used to discriminate which pathway is dominant. When CH₄ diffuses from sediments to the water column, it can be
 125 oxidized by methanotrophic bacteria who preferentially consume CH₄ with ¹²C over ¹³C, resulting in an increase of δ¹³C-CH₄
 126 of the residual CH₄ in the water column (Bastviken et al., 2002). Fractionation models then allow estimating methane
 127 oxidation (MOX) from measurements of δ¹³C-CH₄ of dissolved CH₄ in the water column. Bastviken et al. (2008) report that
 128 30 to 99% of the CH₄ produced in sediments of freshwater lakes can be removed by MOX that is as a significant CH₄ sink in
 129 these water bodies. MOX is known to be inhibited by light (Dumestre et al., 1998) and increases with the presence
 130 suspended particles (Abril et al. 2007) so that MOX might vary between clear and turbid waters (Morana et al. 2020).

131

132 Here, we report a dataset of CO₂, CH₄, and N₂O dissolved concentrations ~~dynamics~~ in four shallow and small urban ponds
 133 (Leybeek, Pêcherries, Silex, and Tenreuken) in the city of Brussels (Belgium) (Fig. 1), ~~with -dData were~~ collected 46 times at
 134 regular intervals (between June 2021 and December 2023) on each pond ~~between June 2021 and December 2023 at a~~
 135 ~~frequency ranging from one (winter) to three (summer) times per month at a single fixed station in each of the four ponds.~~
 136 The air-water diffusive fluxes of CO₂, CH₄, and N₂O were calculated from dissolved concentrations and the gas transfer
 137 velocity, ~~while -and~~ the ebullitive CH₄ fluxes were measured with inverted funnels during 8 deployments (totalling 48 days)
 138 in the four ponds. The ~~¹³C/¹²C ratio of CH₄ (δ¹³C-CH₄)~~ in the sedimentary bubbles and in the water provides additional
 139 information on CH₄ dynamics such as the methanogenesis pathway (acetoclastic or hydrogenotrophic) and ~~methane~~
 140 ~~oxidation (MOX).~~ We test the hypothesis that the two alternative states in shallow lakes (a clear-water state dominated by
 141 macrophytes, or a turbid-water state dominated by phytoplankton) drive differences in the CO₂, CH₄, and N₂O dissolved
 142 concentration and diffusive emissions from the four studied artificial ponds, that have similar depth, surface area, and
 143 catchment urban coverage, and that mainly differ by the phytoplankton-macrophyte dominance. We also test the hypothesis
 144 that the two alternative states in shallow lakes drive differences in the ebullitive CH₄ emissions, water column MOX, and
 145 sedimentary methanogenesis pathway (acetoclastic or hydrogenotrophic) in the four studied ponds. The final objective of the
 146 present work is to determine the relative contribution of CO₂, CH₄, and N₂O to the total GHG emissions in CO₂-eq and to
 147 test the hypothesis that the relative contribution of each GHG differs according to the two alternative states in shallow lakes.

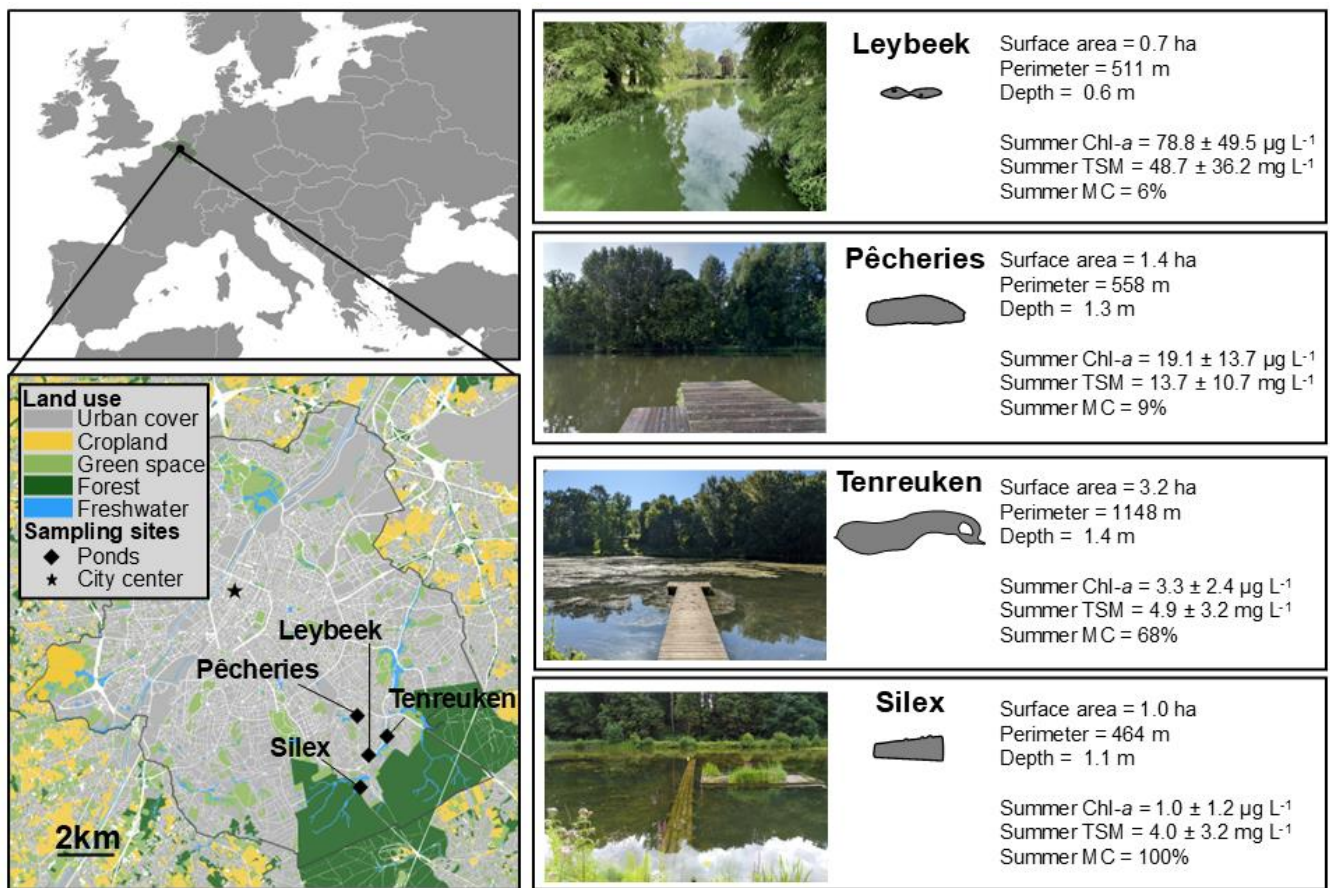


Figure 1: Location of the four sampled ponds in Brussels (Belgium, Europe). Bottom left map shows the metropolitan area of the region of Brussels delineated by the black line and the surrounding region of Flanders in Belgium, showing land cover and sampled urban ponds (black diamonds). The star corresponds to the center of the city (50.8504°N, 4.3487°E). Additional information for each pond is indicated on right panels: shapes of the ponds, surface area (ha), perimeter (m), average depth (m), mean±standard deviation of summer chlorophyll-*a* (Chl-*a*, in $\mu\text{g L}^{-1}$) and summer total suspended matter (TSM, in mg L^{-1}) of periods from 21 June 21 to 21 September 21 in 2021, 2022, 2023, and summer total macrophyte cover (MC, in %) (Table S1).

2. Material and Methods

2.1. Field sampling and meteorological data

Sampling was ~~done~~ carried out from a pontoon, in the four ponds on the same day between 9am and 11am, 46 times on each pond between June 2021 and December 2023 at a frequency ranging from one (winter) to three (summer) times per month at a single fixed station in each of the four ponds. Water was sampled 5cm below the surface with 60ml polypropylene syringes for analysis of dissolved concentrations of ~~gases~~ (CO_2 , CH_4 , and N_2O). Samples for CH_4 and N_2O were transferred from the syringes with a silicone tube into 60 ml borosilicate serum bottles (Weathon), preserved with 200 μl of a saturated solution of HgCl_2 , sealed with a butyl stopper and crimped with aluminium cap, without a headspace, samples were stored at ambient temperature protected from direct light prior to analysis in laboratory and a 2L polyethylene water container for processing at the home laboratory for other variables. Water temperature, specific conductivity, and % O_2 were measured ~~in situ with VWR MU 6100H probe~~. The partial pressure of CO_2 (pCO_2) was measured directly in the field, within 5 minutes of sample collection, with a Li-Cor Li-840 infrared gas analyser (IRGA) based on the headspace technique with 4 polypropylene syringes (Borges et al., 2019). A volume of 30 ml of sample water was equilibrated with 30 ml of atmospheric air within the syringe by shaking vigorously for 5 minutes. The headspace of each syringe was then sequentially injected into the IRGA and a fifth syringe was used to measure atmospheric CO_2 . The final pCO_2 value was computed taking into account

the partitioning of CO₂ between water and the headspace, as well as equilibrium with HCO₃⁻ (Dickson et al., 2007) using water temperature measured in-situ and after equilibration, and total alkalinity (data not shown). Samples for total alkalinity were conditioned, stored and analysed as described by Borges et al. (2019). The ~~Li-Cor 840-IRGA~~ was calibrated ~~before and after each cruise in the laboratory~~ with ultrapure N₂ and a suite of gas standards (Air Liquide Belgium) with CO₂ mixing ratios of 388, 813, 3788 and 8300 ppm. The ~~overall~~-precision of pCO₂ measurements was ±2.0%. ~~Samples for CH₄ and N₂O were transferred from the syringes with a silicone tube in 60 ml borosilicate serum bottles (Weathon), poisoned with 200 µl of a saturated solution of HgCl₂ and sealed with a butyl stopper and crimped with aluminium cap, without a headspace.~~ Water temperature, specific conductivity, and oxygen saturation level (%O₂) were measured in-situ with VWR MU 6100H probe 5cm below the surface. A 2 liter polyethylene water container was filled with surface water for conditioning the samples for other variables at the laboratory in Université Libre de Bruxelles.

Surveys to identify and quantify visually the relative coverage of emerged and submerged macrophytes were conducted in summer 2023 (Table S1). The ~~is~~ resulting list of ~~macrophyte~~ species ~~of macrophytes~~ agreed with past studies in Brussels ponds (Peretyatko et al., 2009).

Three bubble traps were deployed ~~at~~ 50 cm apart for measuring ebullitive CH₄ flux. The bubble traps ~~consiste~~consisted of ~~nt~~ ~~in~~ inverted polypropylene funnels (diameter 23.5 cm) mounted with 60 ml polypropylene ~~syringessyringes~~, with three way stop valves allowing to collect the gas without contamination from ambient air. The polypropylene funnel was ~~and~~ attached with steel rods to a polystyrene float. The volume of gas collected in the funnels was ~~sampled with graduated polypropylene 60 ml syringes measured every 24 hours with 60ml syringes~~. The value of the collected volume of gas was logged, and the gas was ~~stored~~transferred immediately after collection to ~~in~~ pre-evacuated 12 ml vials (Exetainers, Labco, UK) that were stored at ambient temperature protected from direct light ~~for prior to the analysis of CH₄ concentration and δ¹³C-CH₄ in the laboratory~~. The ~~time-series of measurement series~~ were ~~lengthier~~longer at the Silex pond than the other three ponds, because the Silex pond is closed to the public during the week, while the other three ponds are open to the public all the time.

In summer 2023, the bubbles present in the sediment were directly ~~sampled~~collected with bubble traps by physically perturbing the sediment ~~below the traps~~ with a wooden rod. The gas collected in the funnels was stored in pre-evacuated 12 ml vials (Exetainers, Labco, UK) that were stored at ambient temperature protected from direct light prior to the analysis of δ¹³C-CH₄ in the laboratory. These samples are referred hereafter to as from “perturbed sediments.” The samples collected in the bubble traps during the ebullition measurements are referred to as from “trapped bubbles.”

Air temperature, precipitation, wind speed, and atmospheric pressure, were retrieved from <https://wow.meteo.be/en> for the meteorological station of the Royal Meteorological Institute of St-Lambert (50.8408°N, 4.4234°E) in Brussels, located between 2.5 and 5.0 ~~kilometers~~ km from the surveyed ponds. Air temperature, wind speed and atmospheric pressure were averaged over 24 h to obtain a daily mean value. Precipitation was integrated each day to obtain ~~cumulated~~ daily rainfall.

2.2. Laboratory analysis

~~2.1.1.2.2.1.~~ Chlorophyll-*a*, total suspended matter, and dissolved inorganic nutrients

Water was filtered through Whatman GF/F glass microfiber filters (porosity 0.7 µm) with a diameter of 47 mm for total suspended matter (TSM) and Chl-*a*. Filters for TSM were dried in an oven at 50 °C and filters for Chl-*a* were kept frozen (-20 °C). The weight of each filter was determined before and after filtration of a known volume of water using an Explorer™ Pro EP214C analytical microbalance (accuracy ±0.1 mg) for determination of TSM concentration. Chl-*a* concentration was

measured on extracts with 90% acetone by fluorimetry (Kontron model SFM 25) (Yentsch and Menzel, 1963) with a limit of detection of 0.01 $\mu\text{g L}^{-1}$. Filtered water was stored frozen ($-20\text{ }^{\circ}\text{C}$) in 50 ml polypropylene bottles for analysis of dissolved nutrients. Soluble reactive phosphorus (SRP) was determined by the ammonium molybdate, ascorbic acid and potassium antimony tartrate staining method (Koroleff, 1983), with a limit of detection of 0.1 $\mu\text{mol L}^{-1}$. Ammonium (NH_4^+) was determined by the nitroprusside-hypochlorite-phenol staining method (Grasshoff and Johannsen, 1972), with a limit of detection of 0.05 $\mu\text{mol L}^{-1}$. Nitrite (NO_2^-) and nitrate (NO_3^-) were determined before and after reduction of NO_3^- to NO_2^- by a cadmium-copper column, using the Griess acid reagent staining method (Grasshoff and Kremling, 2009), with a detection limit of 0.01 and 0.1 $\mu\text{mol L}^{-1}$, respectively. Concentration of dissolved inorganic nitrogen (DIN) was calculated as the sum NH_4^+ , NO_2^- and NO_3^- concentrations in $\mu\text{mol L}^{-1}$.

2.1.2.2.2. CH_4 and N_2O measurements by gas chromatography and $\delta^{13}\text{C}-\text{CH}_4$ by cavity ring-down spectrometry

Measurements of N_2O and CH_4 concentrations dissolved in water and in the gas samples from bubbles were made with the headspace technique (Weiss 1981) with an headspace volume of (20ml of ultra-pure N_2 (Air Liquid Belgium), Weiss, 1981) and a gas chromatograph (GC) (SRI 8610C) with a flame ionisation detector for CH_4 (with a methanizer for CO_2) and an electron capture detector for N_2O calibrated with CO_2 : CH_4 : N_2O : N_2 gas mixtures (Air Liquide Belgium) with mixing ratios of 1, 10 and 30 ppm for CH_4 , 404, 1018, 3961 ppm for CO_2 , and 0.2, 2.0 and 6.0 ppm for N_2O . The precision of measurement based on duplicate samples was $\pm 3.9\%$ for CH_4 and $\pm 3.2\%$ for N_2O .

The CO_2 concentration is expressed as partial pressure (pCO_2) in parts per million (ppm) and CH_4 as dissolved concentration (nmol L^{-1}), in accordance with convention in existing gas frequently used in topical literature, and because both quantities CH_4 concentration were systematically and distinctly above saturation level (400 ppm and 2-3 nmol L^{-1} , respectively) and pCO_2 values were only five times below saturation out of the 187 measurements. Variations-The of N_2O were modest and concentrations fluctuated around atmospheric equilibrium, so data are presented as percent of saturation level (% N_2O , where atmospheric equilibrium corresponds to 100%). The equilibrium with atmosphere for N_2O was calculated from the average air mixing ratios of N_2O provided by the Global Monitoring Division (GMD) of the National Oceanic and Atmospheric Administration (NOAA) Earth System Research Laboratory (ESRL) (Dutton and Hall, 2023), and using the Henry's constant given by Weiss and Price (1980).

The $\delta^{13}\text{C}-\text{CH}_4$ was measured in the gas of the headspace (20 ml of synthetic air, Air Liquid Belgium) equilibrated with the water sample (total volume 60 ml) for water samples and directly on in the gas stored in Exetainers for gas-samples from the bubble traps. The gas samples were diluted to obtain a final partial pressure of CH_4 in the cavity below 10 ppm (target value of 6 ppm) to fall within the recommended-operational concentration range of the instrument recommended by the manufacturer, prior to injection into a cavity ring-down spectrometer (G2201-Fi, Isotopic Analyzer, Picarro) with a Small Sample Introduction Module 2 (SSIM, Picarro). Data were corrected with curves of $\delta^{13}\text{C}-\text{CH}_4$ as a function of concentration based on two gas standards from Airgas Specialty Gases with certified $\delta^{13}\text{C}-\text{CH}_4$ values of $-23.9\pm 0.3\text{ }‰$ and $-69.0\pm 0.3\text{ }‰$.

2.1.3.2.1.1. Chlorophyll a, total suspended matter, and dissolved inorganic nutrients

Water was filtered through Whatman GF/F glass microfiber filters (porosity 0.7 μm) with a diameter of 47 mm for total suspended matter (TSM) and Chlorophyll a (Chl a). Filters for TSM were dried in the oven at 50°C and filters for Chl a were kept frozen (-20°C). The weight of each filter was determined before and after filtration of a known volume of water using an Explorer™ Pro EP214C analytical microbalance (accuracy: $\pm 0.1\text{ mg}$) for determination of TSM. Filtered water was

stored in 50 ml plastic bottles and frozen (-20°C) for analysis of dissolved nutrients. Chl a was measured on extracts with 90% acetone by fluorimetry (Kontron model SFM 25) (Yentsch and Menzel, 1963) with a limit of detection of $0.01 \mu\text{g L}^{-1}$. Ammonium (NH_4^{+}) was determined by the nitroprusside-hypochlorite-phenol staining method (Grasshoff and Johannsen, 1972), with a limit of detection of $0.05 \mu\text{mol L}^{-1}$. Nitrite (NO_2^{-}) and nitrate (NO_3^{-}) were determined before and after reduction of NO_3^{-} to NO_2^{-} by a cadmium-copper column, using the Griess acid reagent staining method (Grasshoff and Kremling, 2009), with a detection limit of 0.01 and $0.1 \mu\text{mol L}^{-1}$, respectively. Soluble reactive phosphorus (SRP) was determined by the ammonium molybdate, ascorbic acid and potassium antimony tartrate staining method (Koroleff, 1983), with a limit of detection of $0.1 \mu\text{mol L}^{-1}$. Concentration of dissolved inorganic nitrogen (DIN) was calculated as the sum NH_4^{+} , NO_2^{-} and NO_3^{-} concentrations.

2.2.2.3. Calculations

2.2.1.2.3.1. Diffusive GHG emissions

The diffusive air-water CO_2 , CH_4 , or N_2O fluxes (F_G) were computed according to Eq. (1):

$$F_G = k\Delta[G], \quad (1)$$

where k is the gas transfer velocity and $\Delta[G]$ is the air-water gas concentration gradient.

The atmospheric pCO_2 was measured on in the field with the Li-Cor Li-840. For CH_4 , the global average present day atmospheric mixing ratio A constant atmospheric concentration of 1.9 ppm was used (Lan et al., 2024) for CH_4 . The equilibrium with atmosphere for Atmospheric N_2O concentration was calculated from the average air mixing ratios of N_2O provided by the Global Monitoring Division (GMD) of the National Oceanic and Atmospheric Administration (NOAA) Earth System Research Laboratory (ESRL) (Dutton et al., 2017).

k was computed from a value normalized to a Schmidt number of 600 (k_{600}) and from the Schmidt number of CO_2 , CH_4 and N_2O in freshwater according to the algorithms as function of water temperature given by Wanninkhof (1992).

k_{600} was calculated from the parameterization as a function of wind speed of Cole and Caraco (1998).

CH_4 and N_2O emissions were converted into CO_2 equivalents ($\text{CO}_2\text{-eq}$) considering a 100-year timeframe, using global warming potential (GWP) of 32 and 298 for CH_4 and N_2O , respectively (Myrhe et al., 2013).

2.2.2.3.2. Ebullitive flux

Bubble flux ($\text{ml m}^{-2} \text{ d}^{-1}$) measured with the inverted funnels was calculated according to Eq. (2):

$$F_{\text{bubble}} = \frac{V_g}{A \times \Delta t}, \quad (2)$$

where V_g is the volume of gas collected in the funnels (ml), A is the cross-sectional area of the funnel (m^2), Δt is the collection time (d).

A multiple linear regression model of F_{bubble} dependent on water temperature and drops of atmospheric pressure (Δp) was fitted to the data according to Eq. (3):

$$\log_{10}(F_{\text{bubble}}) = \alpha \times T_w + \beta \times \Delta p, \quad (3)$$

where α and β are the slope coefficients of the multiple linear regression model, T_w is the water temperature ($^{\circ}\text{C}$), and Δp quantifies the drops in atmospheric pressure (atm), calculated according to Zhao et al. (2017) in Eq. (4):

$$\Delta p = -\frac{1}{\Delta t} \int_0^t p - p_0 ; \quad \forall p < p_0 , \quad (4)$$

where p is the atmospheric pressure (atm), p_0 a threshold pressure fixed at 1 atm and Δt the time interval between two measurements (d) (Fig. S1).

Ebullitive CH_4 fluxes ($\text{mmol m}^{-2} \text{d}^{-1}$) were calculated according to Eq. (5):

$$E_{\text{CH}_4} = [\text{CH}_4] \times F_{\text{bubble}} , \quad (5)$$

where $[\text{CH}_4]$ is the CH_4 concentration in bubbles (mmol ml^{-1}).

The methane ebullition Q_{10} represents the proportional change in the ebullitive CH_4 flux per 10°C alteration-change in water temperature (DelSontro et al., 2016) and was computed according to Eq. (6):

$$Q_{10} = 10^{10b} , \quad (6)$$

where b is the slope of the linear regression between the logarithm of the ebullitive CH_4 flux (E_{CH_4}) and the water temperature (T_w), and c is the y-intercept, according to Eq. (7):

$$\log_{10}(E_{\text{CH}_4}) = b \times T_w + c , \quad (7)$$

The flux of CH_4 from dissolution of rising bubbles was computed using the model of McGinnis et al. (2006) implemented in the SiBu-GUI graphical user interface (Greinert and McGinnis, 2009).

2.2.3.2.3.3. Methane oxidation

The fraction of CH_4 removed-oxidized (FOX) was calculated with a closed-system Rayleigh fractionation model (Liptay et al., 1998) according to Eq. (8):

$$\ln(1 - \text{FOX}) = \frac{\ln(\delta^{13}\text{C-CH}_4_{\text{initial}} + 1000) - \ln(\delta^{13}\text{C-CH}_4 + 1000)}{\alpha - 1} , \quad (8)$$

where $\delta^{13}\text{C-CH}_4_{\text{initial}}$ is the $^{13}\text{C}/^{12}\text{C}$ ratio signature of dissolved CH_4 as produced by methanogenesis in sediments, $\delta^{13}\text{C-CH}_4$ is the $^{13}\text{C}/^{12}\text{C}$ ratio signature of dissolved CH_4 in-situ, and α is the fractionation factor.

We used a value of 1.02 for α based on laboratory culture experiments carried out at 26°C (Coleman et al., 1981) and field measurements in three Swedish lakes (Bastviken et al., 2002) and one tropical lake (Morana et al., 2015). The α values gathered in the three Swedish lakes were independent of season and temperature according to Bastviken et al. (2002) and were very similar to those derived in a tropical lake by Morana et al. (2015).

For $\delta^{13}\text{C-CH}_4_{\text{initial}}$, we used a value of -69‰ for spring and summer, and -83‰ for fall based on average of measured $\delta^{13}\text{C-CH}_4$ in trapped bubbles (see Sect. 3.5). For winter we used a value of -76‰ corresponding to the average of the fall and spring/summer values.

MOX was ~~indirectly determined~~ computed from FOX and the F_G of CH_4 (F_{CH_4}) according to (Bastviken et al., 2002) ~~in Eq. (9)~~:

$$MOX = F_{CH_4} \times \frac{FOX}{1 - FOX}, \quad (9)$$

2.3.2.4. Statistical analysis

Statistical analysis was conducted with R version 4.4.1. Pearson's linear correlation coefficients and the r^2 coefficient were used to assess relationships between log-transformed variables within each pond and across the dataset, to identify potential pond-specific and overall direct relationships between variables and GHGs. Statistical significance was determined using Fisher's F test and the associated p -value. This approach was also applied to study the relationships between $\delta^{13}C$ - CH_4 , FOX and MOX with $Chl-a$ and TSM . To assess the impact of $Chl-a$ concentration, macrophyte cover in summer, water depth, and lake surface area on diffusive and ebullitive CH_4 fluxes, the ratio of ebullitive CH_4 to total CH_4 flux, and CO_2 and N_2O fluxes, both linear and quadratic relationships were applied to log-transformed averaged data. This approach allowed for the observation of trends between explanatory and dependent variables. For N_2O fluxes, additional explanatory variables included NO_2^- , NO_3^- , NH_4^+ , and DIN concentrations.

A two-way repeated measures analysis of variance (ANOVA) was used to test for differences in categorical variables, with the four seasons and the four ponds serving as independent factors, pond was set as a random effect to account for repeated measurements. A one-way repeated measures ANOVA was used to test for differences in $\delta^{13}C$ - CH_4 from "perturbed sediments" with the four ponds serving as independent factors. After conducting an ANOVA and establishing significant differences among at least two groups ($p < 0.05$), Tukey's Honestly Significant Difference (HSD) post-hoc test was employed to perform pairwise comparisons across all groups. Statistical outcomes are visually represented on boxplots, where upper- and lower-case letters are used to denote significant differences ($p < 0.05$). Different lower- and upper-case letters indicate significant differences between groups.

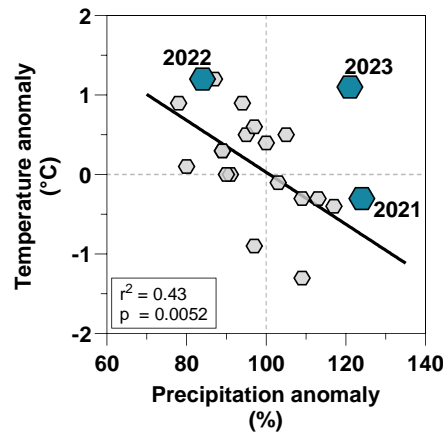
~~and graphs production were conducted utilizing GraphPad Prism v10. Prior to analysis, data underwent log transformation to ensure normality, with Shapiro tests conducted to assess distribution normality. Ordinary one way ANOVA and Pearson's rank correlation were employed to examine differences and correlations among variables. The regressions depicted in the graphs are characterized as linear, exponential, or quadratic, and are explicitly identified when utilized.~~

3. Results and discussion

3.1. Seasonal variations of meteorological conditions and GHG concentrations

Belgium has a west coast marine climate with mild weather year-round, and evenly distributed abundant rainfall totalling on average 837 mm annually for the reference period 1991-2020. The average annual air temperature was 11°C, with summer average of 17.9 °C and winter average of 4.1 °C for the reference period 1991-2020. During the sampling period, from June 2021 to December 2023, water temperature in the surface of the four sampled ponds (Leybeek, Pêcherries, Silex, and Tenreuken; Fig. 1) tracked closely the air temperature that ranged between -1.5 and 30.0°C following the typical seasonal cycle at mid-latitudes in the Northern Hemisphere (Fig. S2). Years 2022 and 2023 were about 1 °C warmer than the average for the period 1991-2020 (11 °C), while year 2021 was closer to the long-term average (Fig. 2). Year 2022 was warmer and drier than 2021 and 2023 (Fig. 2), with positive temperature anomalies observed evenly throughout the year (9 months out of 12) and negative precipitation anomalies in summer, fall and early winter (Fig. S2). ~~Conversely, Year 2021 showed had~~

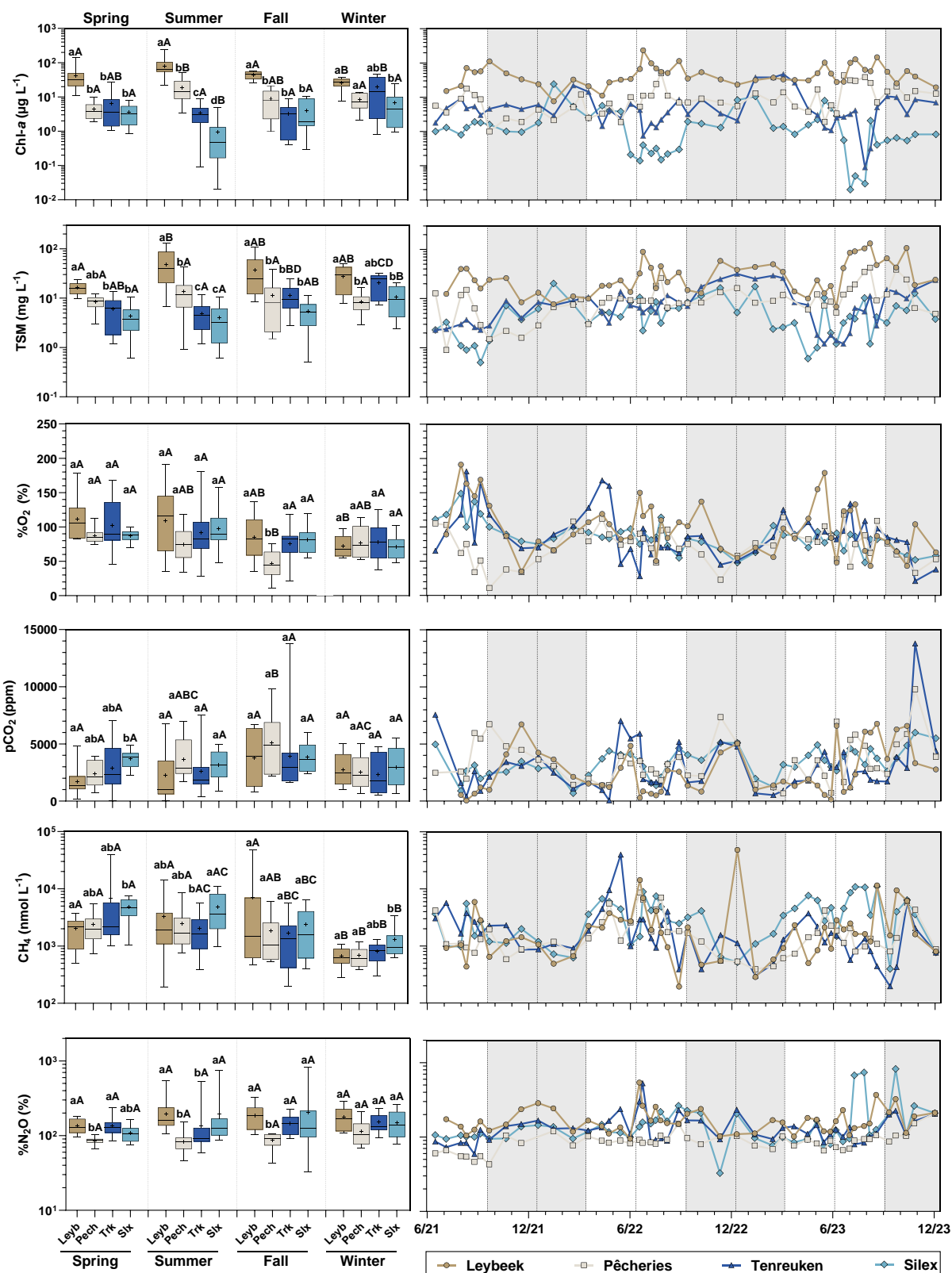
warmer and drier months in June and September, colder and wetter months in July and August, and was overall wetter and colder than 2022 (Fig. 2). Year 2023 was marked by both positive temperature and precipitation anomalies (Fig. S2), resulting in a wetter and warmer year than normal and compared to 2021 and 2022. (Fig. 2). Daily wind speed was generally low ($<1 \text{ m s}^{-1}$) except for a windier period in spring 2022 (up to 5.8 m s^{-1} , corresponding to the Eunice storm) and in fall 2023 (up to 9.7 m s^{-1} , corresponding to the Ciarán storm) (Fig. S2).



348

Figure 2: Temperature anomaly (difference between the average annual temperature and the normal annual temperature for the reference period 1991-2020 (11 °C), in °C) plotted against precipitation anomaly (ratio between annual precipitation and normal annual precipitation for the reference period 1991-2020 (837 mm), in %) from 2003 to 2023 for the reference period 1991-2020 in the city of Brussels (11°C and 837mm). Each small grey hexagon represents values for years from 2003 to 2020 and filled larger blue hexagons represent the years of sampling from this study (2021, 2022 and 2023). Linear regression for years 2003-2020 is shown as by a black solid line ($Y = 3.29 - 0.03 \cdot X$, $n=20$, Table S115). Note the anomalous rainy year in 2023 relative to the pattern as function of temperature for the other years, possibly in response to the strong El Niño event of 2023 (Chen et al., 2024).

The four sampled ponds were situated in the periphery of the city of Brussels, with the Silex pond bordered by the Sonian Forest (Fig. 1). The four ponds are relatively small (0.7-3.2 ha) and shallow (0.60-1.40 m) and have not been drained or dredged since at least 2018 (Table S2). The four studied ponds had significantly different Chl-*a* concentration values during summer, with the Leybeek pond having higher Chl-*a* ($78.8 \pm 49.5 \mu\text{g L}^{-1}$), followed by the Pêcherries pond ($19.1 \pm 13.7 \mu\text{g L}^{-1}$), the Tenreuken pond ($3.3 \pm 2.4 \mu\text{g L}^{-1}$), and the Silex pond ($1.0 \pm 1.2 \mu\text{g L}^{-1}$) (Tukey's HSD test $p \leq 0.0001$ for each pair of comparisons, Figs. 1, 3). The Leybeek and Pêcherries ponds with higher summer Chl-*a* concentration had turbid-water (summer TSM = 48.7 ± 36.2 and $13.7 \pm 10.7 \text{ mg L}^{-1}$, respectively), with high summer Chl-*a* (78.8 ± 49.5 and $19.1 \pm 13.7 \mu\text{g L}^{-1}$, respectively) and high summer TSM (48.7 ± 36.2 and $13.7 \pm 10.7 \text{ mg L}^{-1}$, respectively) concentration values, and undetectable submerged macrophyte cover in summer (Fig. 1, Table S1). Values of Chl-*a* and TSM concentrations were generally higher in the Leybeek pond compared to Pêcherries pond (Fig. 3). The Tenreuken and Silex ponds with lower summer Chl-*a* concentrations had clear-water (summer TSM = 4.9 ± 3.2 and $4.0 \pm 3.2 \text{ mg L}^{-1}$, respectively) with low summer Chl-*a* (3.3 ± 2.4 and $1.0 \pm 1.2 \mu\text{g L}^{-1}$, respectively) and TSM (4.9 ± 3.2 and $4.0 \pm 3.2 \text{ mg L}^{-1}$, respectively) concentration values, and a high total macrophyte cover during summer (68 and 100%, respectively, Fig. 1, Table S1). Values of Chl-*a* were higher in summer than in winter in the turbid-water Leybeek and Pêcherries ponds (Tukey's HSD test $p=0.0107$ for the Leybeek pond, $p=0.0211$ for the Pêcherries pond) related to summer algal blooms. Values of Chl-*a* were higher in winter than in summer in the clear-water Tenreuken and Silex ponds (Tukey's HSD test $=0.0296$ for the Tenreuken pond, $p=0.0056$ for the Silex pond). The low summer time values of Chl-*a* and TSM concentrations in the Silex and Tenreuken ponds are probably related to competition for inorganic nutrients from macrophytes, with the Silex pond showing lower summer Chl-*a* (Tukey's HSD test $p<0.0001$), lower summer TSM concentrations (Tukey's HSD test $p<0.0001$) and higher summer total macrophyte cover compared to the Tenreuken pond (Fig. 1).



377

378 | Figure 3: Seasonal variations of Chlorophyll-a (Chl-a, in $\mu\text{g L}^{-1}$), total suspended matter (TSM, in mg L^{-1}), oxygen saturation
379 | ($\%\text{O}_2$, in %), partial pressure of CO_2 (pCO_2 in ppm), dissolved CH_4 concentration (CH_4 , in nmol L^{-1}), and N_2O saturation level
380 | ($\%\text{N}_2\text{O}$, in %) in four urban ponds (Leybeek (Leyb), Pêcherie (Pech), Tenreken (Trk), and Silex (Slx)) in the city of Brussels
381 | (Belgium) from June 2021 to December 2023. Box plots show median (horizontal line), mean (cross), and 25–75% percentiles (box
382 | limits). Whiskers extend from minimum to maximum values. White and grey bands in the graphs on the right correspond to the
383 | autumn/winter and spring/summer periods, respectively, and dotted vertical bars represent the first days of each season. ANOVA
384 | results of the multiple comparison between boxplots are summarized in Tables S4 and S5. Different lower-case letters indicate
385 | significant differences between ponds within a season and different upper-case letters indicate significant differences between
386 | seasons for a given pond. ANOVA results of the multiple comparison between boxplots are summarized in Table S6.

387 The %O₂ values ranged from 11 to 191% (Fig. 3). The highest %O₂ values in the four ponds were observed in spring and
 388 summer compared to fall and winter owing to aquatic primary production. In summer, ~~the highest average~~ %O₂ was
 389 ~~observed~~ statically higher in the Leybeek pond (109±46 %) characterized by higher Chl-*a* concentration compared to the
 390 Pêcherries pond (75±23 %) (Tukey's HSD test p=0.0037)~~that was characterized by the highest phytoplankton biomass as~~
 391 ~~indicated by the Chl-*a* concentration~~. The lowest average %O₂ was observed in fall in the Pêcherries pond (46±22 %) and was
 392 statistically lower than in the Leybeek (85±34%, Tukey's HSD test p=0.0302), Tenreuken (76±26 %, Tukey's HSD test
 393 p=0.0488), and Silex ponds (81±19 %, Tukey's HSD test p=0.0132).

394 The pCO₂ values ranged from 40 to 13,804 ppm (Fig. 3), ~~within the range of values typically observed in ponds (Holgerson~~
 395 ~~and Raymond, 2016; Peacock et al., 2019; Audet et al., 2020)~~. Undersaturation of CO₂ with respect to atmospheric
 396 equilibrium was only observed on five occasions out of the 187 measurements, three times in the turbid-water Leybeek pond
 397 in summer (40 ppm on 13 August 2021, 220 ppm on 27 June 2022 and 149 ppm on 13 June 2023), and twice in the clear-
 398 water Tenreuken pond in spring and summer (383 ppm on 13 August 2021 and 55 ppm on 2 May 2022). ~~Minimal~~-Low
 399 values of pCO₂ were generally observed in spring and summer probably due to ~~intense~~ uptake of CO₂ by primary production
 400 from either phytoplankton or submerged macrophytes. ~~Maximal~~-High values of pCO₂ were observed in fall ~~in the four ponds~~
 401 ~~and probably reflect the~~ ~~due to~~ release of CO₂ from degradation of organic matter due to ~~the~~ senescence of phytoplankton or
 402 macrophytes (Fig. 3). A general control of pCO₂ by biological activity (primary production and respiration) was confirmed
 403 by the strong negative correlation with %O₂ observed in all four ponds (*e.g.* ~~Holgerson, 2015~~), as well as a positive
 404 correlation with DIN observed in three ponds, and a positive correlation with SRP ~~was~~ observed in ~~the two clear-water~~ ponds
 405 (Table S3; ~~Figs S3, S4, S5, S6~~). A negative correlation between pCO₂ and Chl-*a* was only observed in the turbid-water
 406 Leybeek pond (Table S3; ~~Fig S5~~), which showed the highest average Chl-*a* concentration, and no correlation was found in
 407 clear-water ponds, where aquatic primary production was presumably mainly related to submerged macrophytes (Table S3;
 408 ~~Figs S3, S4~~). In all four ponds, pCO₂ strongly correlated ~~positively~~ to precipitation (Table S3; ~~Figs S3, S4, S5, S6~~)
 409 suggesting a control of external inputs of carbon either as organic carbon sustaining internal degradation of organic matter or
 410 as soil CO₂ (*e.g.* ~~Marotta et al., 2011~~).

411 The CH₄ dissolved concentrations ranged from 194 to 48,380 nmol L⁻¹ (Fig. 3), ~~within the range of values typically observed~~
 412 ~~in ponds (Holgerson and Raymond, 2016; Peacock et al., 2019; Audet et al., 2020)~~. ~~The dissolved CH₄ concentration was~~
 413 ~~generally higher in spring and summer than fall and winter~~. Dissolved CH₄ concentration was positively correlated to water
 414 temperature in all four ponds (Table S3; ~~Figs S3,S4,S5,S6~~), most probably reflecting the increase of sedimentary
 415 methanogenesis with temperature (Schulz and Conrad, 1996), ~~with higher dissolved CH₄ concentrations observed in spring~~
 416 ~~(3160±5989 nmol L⁻¹) and summer (3979±2993 nmol L⁻¹) than in fall (2645±7315 nmol L⁻¹) and winter (868±601 nmol L⁻¹)~~
 417 ~~(Tukey's HSD test: spring versus fall, p=0.0954; spring versus winter, p<0.0001; summer versus fall, p=0.0154; summer~~
 418 ~~versus winter, p<0.0001)~~. In individual ponds, dissolved CH₄ concentration was ~~sometimes~~ negatively correlated to
 419 precipitation ~~and, SRP, DIN in the Pêcherries pond (Table S3; Fig S6), TSM, or Chl-*a* concentrations~~ and positively
 420 correlated to SRP in the Silex pond (Table S3; Fig S4). These relationships between CH₄ and other variables probably
 421 indirectly reflecting the seasonal variations of these ~~other~~ variables that ~~showed correlations with temperature, as DIN was~~
 422 ~~negatively correlated to temperature in the Pêcherries pond (r²=0.11, p=0.0028), and SRP was positively correlated to~~
 423 ~~temperature in the Silex pond (r²= 0.10, p=0.0103)~~. ~~were minimal in summer when CH₄ was maximal presumably mainly in~~
 424 ~~response to temperature increase (Table S3)~~. A negative correlation between Dissolved CH₄ concentration was negatively
 425 correlated to ~~and~~ Chl-*a* ~~was observed~~ in the Silex pond (Table S3; Fig S4); and ~~to a negative correlation between CH₄ and~~
 426 TSM ~~was observed~~ in the Tenreuken pond (Table S3; Fig S3). These relationships probably reflect the negative relationship

between Chl-*a* and temperature in the Silex pond ($r^2=0.13$, $p=0.0008$) and the negative relationship between TSM and temperature in the Tenreuken pond ($r^2=0.36$, $p<0.0001$) because of the primary production from macrophytes peaks in summer in the two clear-water ponds. Both are clear water ponds where Chl *a* or TSM concentrations were particularly low in summer (Fig. 3).

The correlations between pCO₂ and precipitation, and between dissolved CH₄ concentration and temperature observed in all the four ponds individually were also observed when pooling together the data for all four ponds ("All" in Table S3; Fig S7). The slopes of these correlations were not significantly different between ponds and were not correlated with This suggested that in the four sampled ponds the effect of precipitation on pCO₂ and of temperature on dissolved CH₄ concentration outweighed other potential effects that could have arisen from differences in surface area, depth, or dominance of type of primary producers (phytoplankton or macrophyte) (Table S6) in explaining seasonal variations. These results suggest that the effect of precipitation on pCO₂ and the impact of temperature on dissolved CH₄ concentration outweigh other factors in explaining seasonal variations.

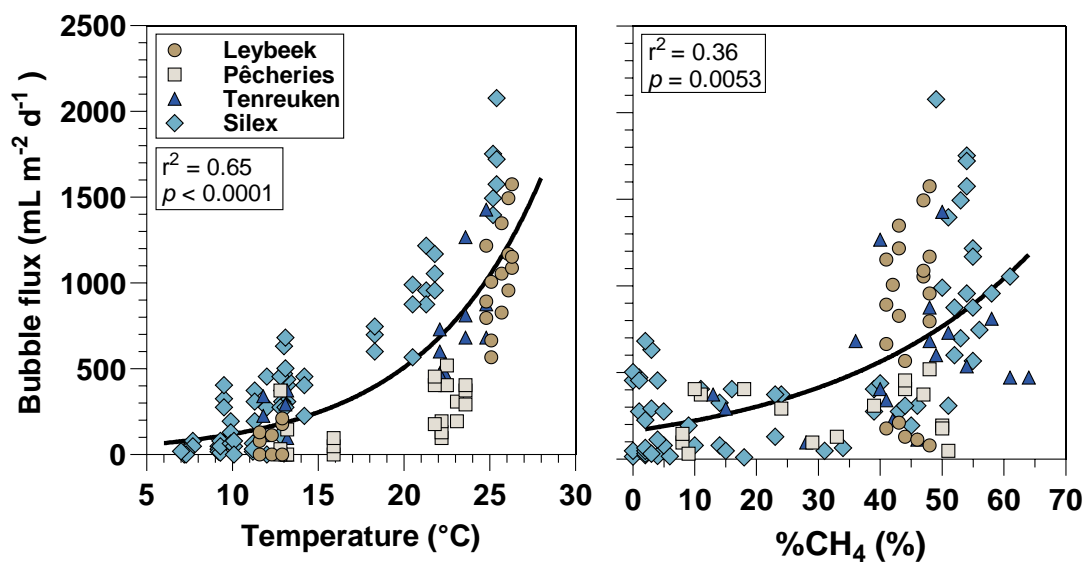
The %N₂O values ranged from 32 to 826% (Fig. 3), within the range of values observed in other ponds (Audet et al., 2020; Rabaey and Cotner, 2022). The %N₂O values did not show clear-significant seasonal variations in any of the four sampled ponds (ANOVA $F(3,174)=1,127$, $p=0.4091$) (Fig. 3). In individual ponds, %N₂O correlated negatively to temperature in the (Tenreuken pond) or and Chl-*a* in the (Silex pond,) and or positively to SRP in the (Silex pond) and TSM concentration in the (Tenreuken pond) (Table S3; Fig S3, S4) concentrations. We do not have a clear explanation for these correlations that might be spurious (Table S3). The correlations with Chl-*a* and TSM were surprisingly since they were observed in the two clear-water ponds and might indirectly reflect seasonal variations (with minimal values of these two quantities in summer). More surprisingly, %N₂O was not correlated with DIN (Table S3; Fig S3, S4, S5, S6) nor with individual forms of DIN (NH₄⁺, NO₂⁻, NO₃⁻) in the four ponds individually or when all the data were pooled together for the individual forms of DIN (Table S3; Fig S7). However, when all the data were pooled together, %N₂O correlated positively to DIN (Table S3), but not with individual forms of DIN (NH₄⁺, NO₂⁻, NO₃⁻). In a previous study of the variation of GHGs in 22 urban ponds in the city of Brussels sampled only once during each season, %N₂O correlated positively with DIN, NH₄⁺, NO₂⁻, and NO₃⁻. The range of variation of DIN and %N₂O across these 22 ponds (2 to 625 μmol L⁻¹ for DIN, and 0 to 10,354% for %N₂O) was higher wider than the one observed in the present study of only four ponds (1 to 135 μmol L⁻¹ for DIN, and 32 to 826% for %N₂O) (Fig. S8). The four ponds studied here are located at the periphery of the city and most probably receive less atmospheric nitrogen deposition than closer to the city center. A lower atmospheric nitrogen deposition in the periphery than in the city center is consistent with the correlation between %N₂O and atmospheric nitrogen dioxide (NO₂), and the correlation between %N₂O and the distance from the city center (Fig. S8); as shown in our previous study by the correlation between %N₂O and DIN in the 22 sampled ponds and atmospheric nitrogen dioxide (Bauduin et al., 2024). Atmospheric nitrogen deposition has been shown to enhance denitrification and N₂O production in lakes (McCrackin and Elser, 2010; Palacin-Lizarbe et al., 2020).

The relationships between GHG dissolved concentrations and other variables were similar in clear-water macrophyte-dominated ponds and turbid-water phytoplankton-dominated ponds. pCO₂ was positively correlated with precipitation, and dissolved CH₄ concentration was positively correlated with temperature, while no significant correlation was found between %N₂O and other variables in the four ponds taken individually. The negative correlation between pCO₂ and %O₂ reflected

the photosynthesis-respiration balance independently from the community driving aquatic primary production (macrophytes in clear-water ponds and phytoplankton in turbid-water ponds).

3.2. Drivers of bubble flux

The bubble flux measured with inverted funnels in the four sampled ponds in the city of Brussels ranged between 0 and 2078 ml m⁻² d⁻¹ and strongly increased with water temperature (Fig. 4) and were overall higher in summer (837±434 mL m⁻² d⁻¹) than in spring (198±170 mL m⁻² d⁻¹) and fall (106±63 mL m⁻² d⁻¹) (Tukey’s HSD test p<0.0001 for summer versus spring and summer versus fall). The bubble flux values in the four sampled ponds in the city of Brussels were within the range of values reported in lentic systems of equivalent size by Wik et al. (2013) (0 to 2772 mL m⁻² d⁻¹), Delsontro et al. (2016) (11 to 748 mL m⁻² d⁻¹) and Ray and Holgerson (2023) (0 to 2079 mL m⁻² d⁻¹). Given the shallowness of the sampled systems (<1.5 m, Fig. 1) we assume that sediments experience the same temperature as surface waters. The CH₄ content of the bubbles also increased with bubble flux (Fig. 4). The mean CH₄ content of the bubbles in the four sampled ponds in the city of Brussels was 31±21%, and comparable to the values obtained by Wik et al. (2013) (35±25%), Delsontro et al. (2016) (58±25%) and Ray and Holgerson (2023) (25±13%) in lentic systems of equivalent size. The CH₄ content of the bubbles increased with bubble flux (Fig. 4). These patterns between bubble flux and temperature and %CH₄ were most probably related to the strong dependence of methanogenesis on temperature (Schulz and Conrad, 1996). As temperature increases, the concomitant increase of methanogenesis with temperature leads to the build-up of gas bubbles in sediments that are richer in CH₄, and consequently to higher bubble fluxes with a higher CH₄ content at higher temperatures.

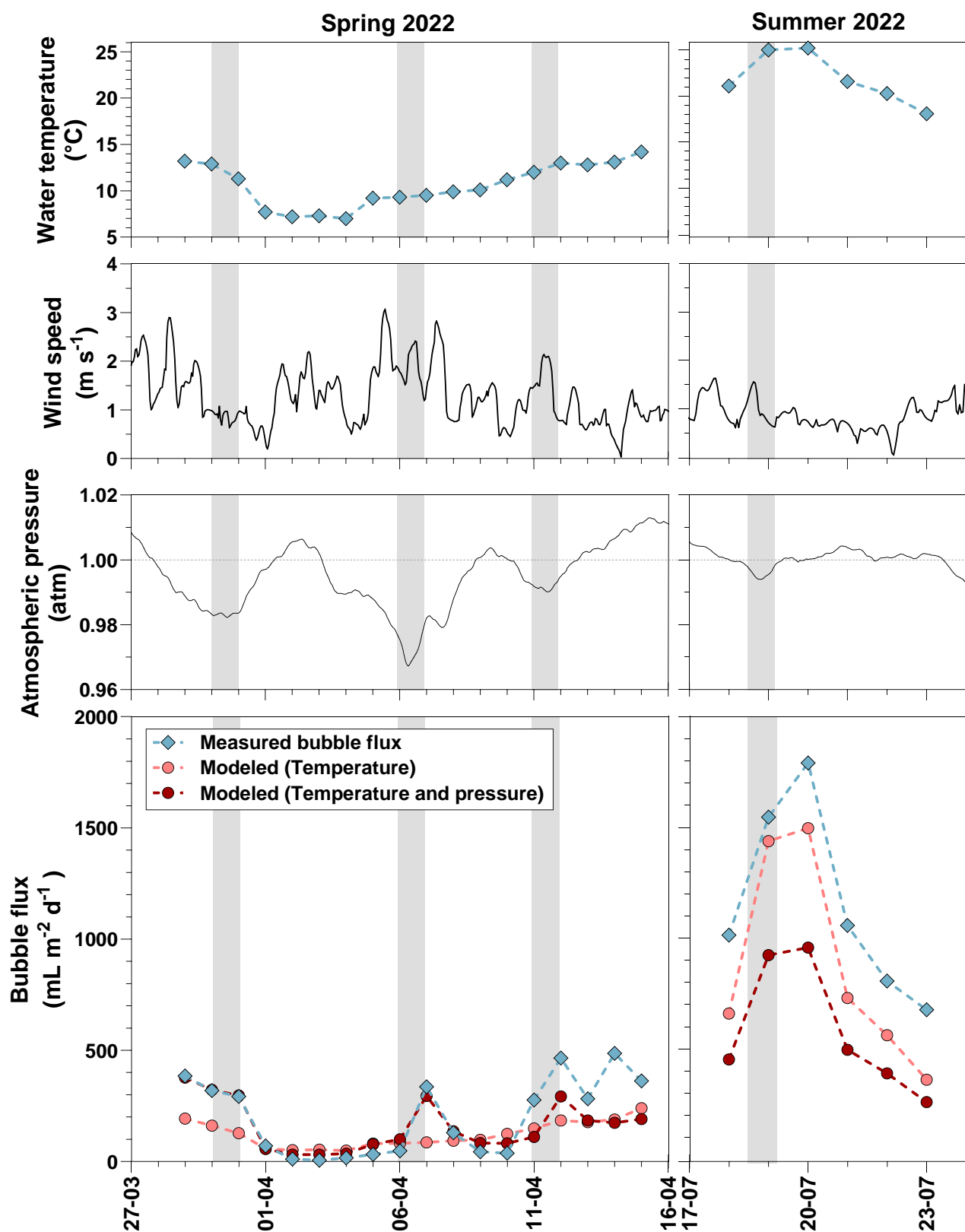


482

Figure 4: Bubbles flux (ml m⁻² d⁻¹) as a function of water temperature (°C) and the relative CH₄ content in bubbles (%CH₄, in %) in four urban ponds (Leybeek, Pêcherries, Tenreuken, and Silex) in the city of Brussels (Belgium). Bubbles fluxes were measured with three bubble traps in spring, summer, and fall of 2022 and 2023, totalling 8 days in the Leybeek, Pêcherries, and Tenreuken ponds and 24 days in the Silex pond. Given the shallowness of the sampled systems (<1.5 m, Fig. 1) we assume that sediments experience the same temperature as surface waters. Solids lines represent exponential regression fit of bubble flux as function of temperature ($Y = 28 \cdot e^{0.14 \cdot X}$, n=139 (Table S5), and as function of relative CH₄ content in the bubbles ($Y = 164 \cdot e^{0.03 \cdot X}$, n=123) (Table S11).

Bubbling events are known to also be triggered by a decrease of hydrostatic pressure on the sediments due to water level fluctuations or changes in atmospheric pressure. Drops in atmospheric pressure have been documented to trigger bubble fluxes from lake sediments (Tokida et al., 2007; Scandella et al., 2011; Varadharajan and Hemond, 2012; Wik et al., 2013; Taoka et al., 2020; Zhao et al., 2021). The bubble fluxes were measured during more lengthy series at the Silex pond than

the other three ponds for logistical reasons allowing investigating in more the detail the effects of temperature and atmospheric pressure variations on bubble fluxes. In spring 2022, the bubble flux at the Silex pond increased during events of drops in atmospheric pressure (depressions) (Fig. 5). There was no relation between wind speed and peaks of bubble flux ($r^2 = 0.01$, $p=0.4629$) as shown in Gatun Lake (Keller and Stallard, 1994), suggesting a more important role of changes of atmospheric pressure than wind speed in the Silex pond in spring 2022. ~~In summer 2022, the bubble flux at the Silex pond~~ was higher in summer ($1152 \pm 433 \text{ mL m}^{-2} \text{ d}^{-1}$) than during spring ($198 \pm 170 \text{ mL m}^{-2} \text{ d}^{-1}$) (Tukey's HSD test $p < 0.0001$), and the temporal changes tracked those of water temperature. The bubble flux was modelled as function of temperature alone or as function of both temperature and pressure changes (Figs. 5, ~~and S93~~). The inclusion of the term of pressure drops in addition to temperature improved the performance of the model compared to the original data, for periods of low temperature ($< 15^\circ\text{C}$) but not for warmer periods ($> 15^\circ\text{C}$) (Figs. 5, ~~and S93~~) when bubbling fluxes ~~are~~ were quantitatively more important. The inclusion of the term of pressure changes only improved the performance of the model compared to the original data very marginally when comparing the full temperature range ($< 15^\circ\text{C}$ and $> 15^\circ\text{C}$) (Fig. S93), showing that the intensity of bubble flux was mainly driven by temperature change at yearly scales, in agreement with previous studies (e.g. Wik et al., 2013; DelSontro et al., 2016; Aben et al., 2017; Ray and Holgerson, 2023).

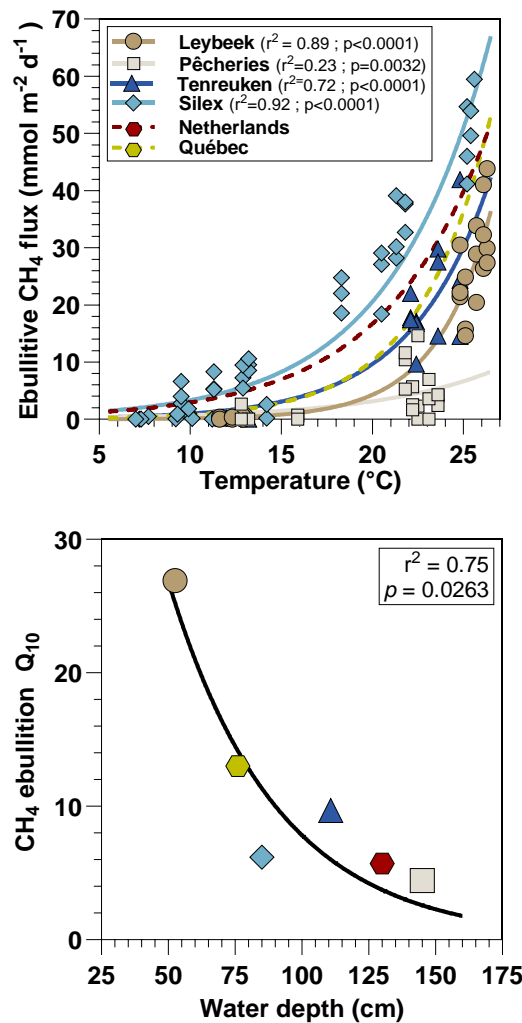


508

509 | Figure 5: Water temperature (°C), wind speed (m s⁻¹), atmospheric pressure (atm), and measured and modeled bubbles flux (mL m⁻² d⁻¹) in the Silex pond from the 29 March 2022 to the 15 April 2022 and from the 18 July 2022 to the 23 July 2022. The bubbles
510 |
511 | flux was modelled from a fit to data based on temperature alone and from both temperature and drops in atmospheric pressure.

512 **3.3. Drivers of methane ebullitive fluxes**

513 Ebullitive CH₄ fluxes in the four ponds ranged between 0 and 59 mmol m⁻² d⁻¹, within the range reported in lentic systems
514 (e.g. Deemer and Holgerson, 2021) and were positively related to temperature (Fig. 6) as shown previously in other small
515 lentic systems (e.g. Wik et al., 2013; DelSontro et al., 2016; Aben et al., 2017; Ray and Holgerson, 2023; Rabaey and
516 Cotner, 2024). The fitted relations between ebullitive CH₄ fluxes and temperature were specific to each pond and
517 encompassed the fitted relations established in similar systems: four small ponds in Québec (DelSontro et al., 2016) and a
518 small urban pond in the Netherlands (Aben et al., 2017). The Q₁₀ of CH₄ ebullition values ranged between 4.4 in the deeper
519 Pêcherries pond and 26.9 in the shallower Leybeek pond, respectively (Table S7). The Q₁₀ of CH₄ ebullition in the four
520 studied ponds of the city of Brussels, in Québec (DelSontro et al., 2016), and in the Netherlands (Aben et al., 2017) were
521 negatively related to water depth (Fig. 6). An increase in water temperature leads to a smaller increase in CH₄ ebullitive
522 fluxes (lower Q₁₀) in deeper ponds as the impact of hydrostatic pressure on sediments is higher in deeper ponds compared to
523 shallow ponds, restricting bubble formation and release (e.g. DelSontro et al., 2016).



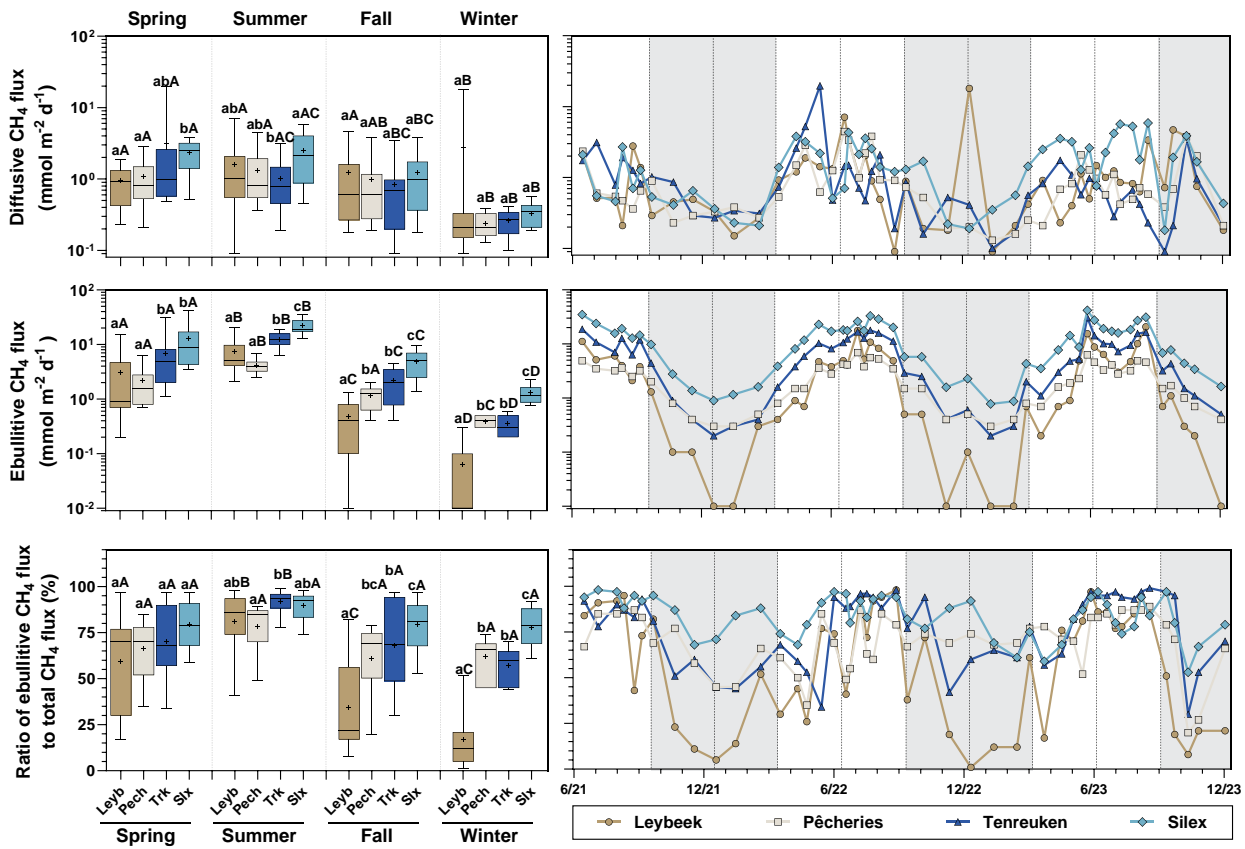
524

525 **Figure 6:** Measured ebullitive CH₄ fluxes (mmol m⁻² d⁻¹) as function of water temperature (°C) in four urban ponds (Leybeek,
526 Pêcherries, Tenreuken, and Silex) in the city of Brussels (Belgium), in spring, summer, and fall of 2022 and 2023, totalling 8 days in
527 the Leybeek, Pêcherries, and Tenreuken ponds and 24 days in the Silex pond, with three bubble traps. Dashed-Solid lines represent
528 exponential fit for the Leybeek ($Y = 0.01 \cdot e^{0.32 \cdot X}$, n=22), Pêcherries ($Y = 0.16 \cdot e^{0.15 \cdot X}$, n=22), Tenreuken ($Y = 0.10 \cdot e^{0.23 \cdot X}$,
529 n=19), Silex ($Y = 0.54 \cdot e^{0.18 \cdot X}$, n=72) ponds the four urban ponds in the city of Brussels (Table S3) and solid- (Table S76) dashed
530 lines represent exponential fit established in similar systems: four small ponds in Québec ($Y = 0.06 \cdot e^{0.25 \cdot X}$) (DelSontro et al.,
531 2016) and a small urban pond in the Netherlands ($Y = 0.51 \cdot e^{0.17 \cdot X}$) (Aben et al., 2017). Each exponential curve allows to

532 determine a Q_{10} of CH_4 ebullition, plotted against water depth; ~~dashed~~ **solid** line represents exponential regression fit ($Y = 92 \cdot$
 533 $e^{-0.02 \cdot X}$, $n = 6$) (Table S110).

534 3.4. Relative contribution of methane ebullitive and diffusive fluxes

535 Diffusive CH_4 fluxes computed from **dissolved** CH_4 concentration and k derived from wind speed ranged between 0.1 and
 536 $19.7 \text{ mmol m}^{-2} \text{ d}^{-1}$ (Fig. 7) **within the range reported in lentic systems (e.g. Deemer and Holgerson, 2021)**. The diffusive CH_4
 537 fluxes tended to be higher in summer and spring than in fall and winter owing to the strong positive dependency between
 538 CH_4 and water temperature (Fig. 3; Table S32). In addition, wind speed only showed small seasonal variations during
 539 sampling, **ranging on average between** ($0.6 \pm 0.6 \text{ m s}^{-1}$ in spring, $0.3 \pm 0.2 \text{ m s}^{-1}$ in summer, $0.7 \pm 0.7 \text{ m s}^{-1}$ in fall, and $0.6 \pm 0.2 \text{ m}$
 540 s^{-1} in winter) (Fig. 3). Ebullitive CH_4 fluxes were calculated from the relations with temperature for each pond given in
 541 Figure 6 from the temperature data coincident with the diffusive CH_4 fluxes (Fig. 7). ~~This~~ **The resulting calculated ebullitive**
 542 **CH_4 fluxes**– allowed to compare and integrated seasonally both components of CH_4 emissions to the atmosphere, and to
 543 calculate the relative contribution of ebullition to total (diffusive+ebullitive) CH_4 emissions.



544

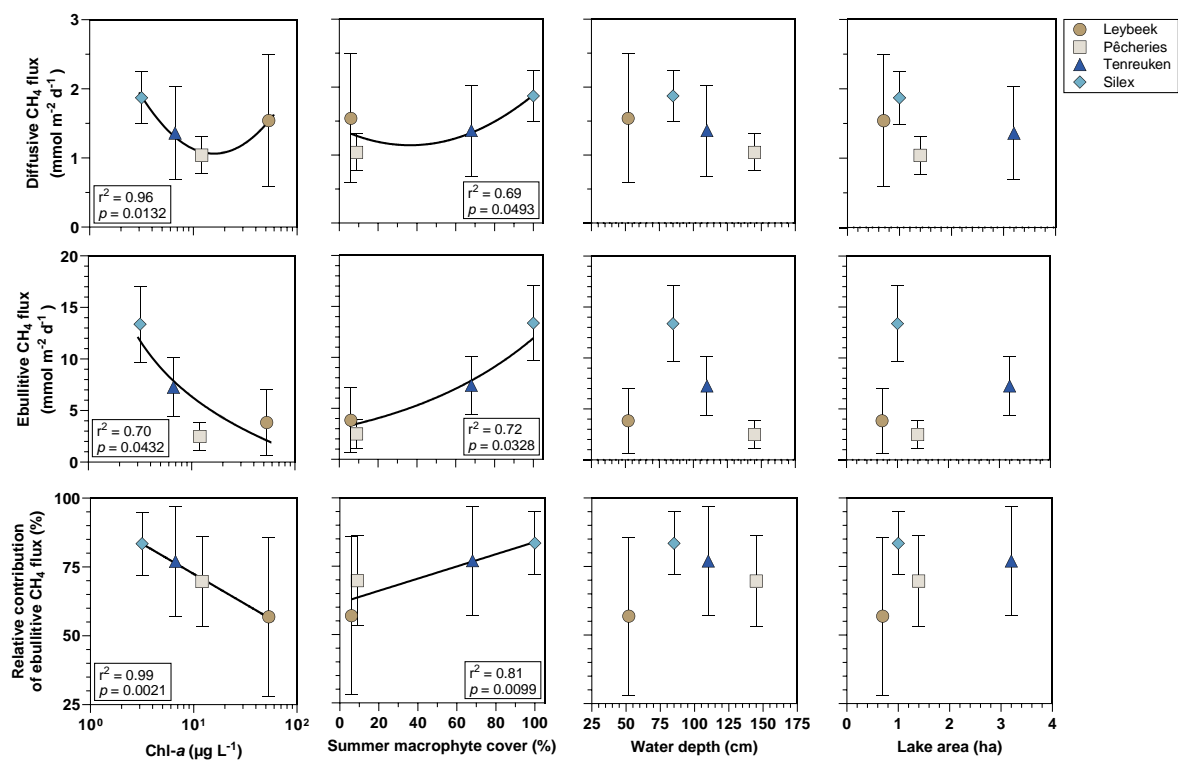
545 Figure 7: Seasonal variations of diffusive and ebullitive CH_4 fluxes ($\text{mmol m}^{-2} \text{ d}^{-1}$), and the ratio of ebullitive CH_4 flux to total
 546 (ebullitive+diffusive) CH_4 flux (%) in four urban ponds (Leybeek (Leyb), Pêcherries (Pech), Tenreuken (Trk), and Silex (Slx)) in the
 547 city of Brussels (Belgium) from June 2021 to December 2023. Diffusive fluxes were calculated from CH_4 concentration and gas
 548 transfer velocity derived from wind speed. Ebullitive CH_4 fluxes were calculated from the relations with temperature for each
 549 pond (Fig. 6; Table S73) from the temperature data coincident with the diffusive CH_4 fluxes. Box plots show median (horizontal
 550 line), mean (cross), and 25–75% percentiles (box limits). Whiskers extend from minimum to maximum values. White and grey
 551 bands in the graphs on the right correspond to the autumn/winter and spring/summer periods, respectively, and dotted vertical
 552 bars represent the first days of each season. ~~ANOVA results of the multiple comparison between boxplots are summarized in~~
 553 ~~Table S6.~~ **ANOVA results of the multiple comparison between boxplots are summarized in Tables S4 and S5. Different lower-case**
 554 **letters indicate significant differences between ponds within a season and different upper-case letters indicate significant**
 555 **differences between seasons for a given pond.**

556 The relative contribution of ebullition to total CH_4 emissions ranged between 1 and 99% in the four sampled ponds in the
 557 city of Brussels (Fig. 7), **within the range reported in lentic systems (e.g. Deemer and Holgerson, 2021)**. Owing to the strong

dependency of ebullitive CH₄ fluxes to temperature (Table S7; Fig. 6), the mean relative contribution of ebullition to total CH₄ emissions for all data pooled together was higher in summer (85±7 %) compared to spring (69±14 %, Tukey's HSD test $p=0.0104$), fall (61±18 %, Tukey's HSD test $p<0.0001$), and winter (53±8 %, Tukey's HSD test $p<0.0001$) ~~was highest in summer, above 75% in all ponds~~ (Fig. 7). This finding is consistent with other studies showing that ebullitive CH₄ fluxes can account for more than half of total CH₄ emissions in small and shallow lentic systems (e.g. Wik et al., 2013; Deemer and Holgerson, 2021; Ray and Holgerson, 2023; Rabaey and Cotner, 2024). The relative contribution of ebullition to total CH₄ emissions was lowest during the other seasons, especially in the Leybeek pond (Fig. 7). Owing to the strong dependency of ebullitive CH₄ fluxes to temperature, the relative contribution of ebullition to total CH₄ emissions was related to temperature in the four ponds (Fig. S10)-, as previously also shown in Québec ponds (DelSontro et al., 2016) ~~(Fig. S4)~~.

The values of Q₁₀ of diffusive CH₄ fluxes were lower than those for ebullitive CH₄ fluxes, less variable (1.2 in the Pêcherries pond to 2.9 in the Silex pond), and less statistically significant (Table S74). Other studies have also ~~observed-reported~~ higher Q₁₀ for ~~ebullitive-CH₄ ebullition flux~~ than for CH₄ diffusion in ~~lakes-and-ponds~~ lentic systems (DelSontro et al., 2016; Xun et al., 2024). The lower dependence to temperature of CH₄ diffusion compared to CH₄ ebullition might be related to a lower relative change of CH₄ concentrations and k to temperature change. CH₄ concentrations in surface water are very strongly affected by MOX (see hereafter). A relative increase of CH₄ production in sediments by methanogenesis will lead to a stronger increase of CH₄ emission by ebullition than by diffusion because of a mitigation by MOX on CH₄ diffusion. Additionally, k depends on wind speed, ~~but: t~~ the warmer periods of the year (summer) tended to be less windy ($\sim 0.3 \text{ m s}^{-1}$) ~~and with lower k values~~ than the other seasons ($>0.6 \text{ m s}^{-1}$) also contributing to lower dependence on temperature of CH₄ diffusion compared to ebullition ~~on temperature~~ and lower Q₁₀ values.

The annual averaged diffusive and ebullitive fluxes of CH₄ in the four ponds in the city of Brussels were plotted against Chl-*a* concentration, total macrophyte cover in summer, water depth, and lake surface area (Fig. 8) that are frequent predictors of variations of CH₄ fluxes among lakes (Holgerson and Raymond, 2016; DelSontro et al., 2018; Deemer and Holgerson, 2021; Casas-Ruiz et al., 2021; Borges et al., 2022). The annual diffusive CH₄ flux was significantly lower in the slightly deeper Pêcherries pond (130 cm depth) than the two slightly shallower ponds (Leybeek (60 cm depth) and Silex (110 cm depth) ponds) (Tukey's HSD test $p=0.0007$ for Pêcherries versus Leybeek, $p<0.0001$ for Pêcherries versus Silex), and the annual ebullitive CH₄ flux was significantly lower in the Pêcherries pond than the Silex pond (Tukey's HSD test $p<0.0001$) but was not significantly different than the Leybeek pond (Tukey's HSD test $p=0.3847$). No other significant differences in annual diffusive and ebullitive CH₄ fluxes related to water depth or surface area were observed. The narrow range of variation of water depth (50 to 150 cm) and surface area (0.7 to 3.2 ha) could explain the lack of a clear decrease of diffusive and ebullitive CH₄ fluxes with increasing depth or surface that are frequent predictors of variations of CH₄ fluxes among ponds (e.g. Holgerson, 2015; Holgerson and Raymond, 2016; Ray et al., 2023; Theus et al., 2023) and lakes (e.g. Kankaala et al., 2013; DelSontro et al., 2018; Deemer and Holgerson, 2021; Casas-Ruiz et al., 2021; Borges et al., 2022). ~~The annual diffusive and ebullitive CH₄ fluxes in the four studied ponds did not show a clear relation with depth and surface area (Fig. 8) that probably reflected the narrow range of variation of these variables (50 to 150 cm for water depth and 0.7 to 3.2 ha for lake surface area).~~ Correlations between CH₄ fluxes and depth or lake surface area have been shown among lakes across much larger ranges of variation of lake depth (Borges et al., 2022) and surface area (Kankaala et al., 2013; Holgerson and Raymond, 2016; Casas-Ruiz et al., 2021).



595

596 **Figure 8:** Mean diffusive and ebullitive CH₄ fluxes (mmol m⁻² d⁻¹) and mean ratio of ebullitive CH₄ flux to total
 597 (diffusive+ebullitive) CH₄ flux (%) versus chlorophyll-*a* (Chl-*a*, in μg L⁻¹), total macrophyte cover in summer (%), water depth
 598 (cm), and lake surface area (ha) in four ponds (Leybeek, Pêcherries, Tenreuken, and Silex) in the city of Brussels (Belgium) from
 599 June 2021 to December 2023. Error bars indicate the standard deviation. Dashed lines indicate trends in relationship between
 600 variables (Table S115).

601 The annual ebullitive CH₄ fluxes were higher in the two clear-water ~~lakes~~ ponds (7.3±2.9 and 13.4±3.7 m⁻² d⁻¹ in the
 602 ~~Tenreuken and Silex~~ ponds, respectively) (~~Tenreuken and Silex~~) than the two turbid-water ~~lakes~~ ponds (3.8±3.2 and 2.5±1.4
 603 m⁻² d⁻¹ in the Leybeek and Pêcherries ponds, respectively) (Tukey's HSD test p<0.0001 for each comparison between a clear-
 604 water pond and a turbid-water pond). The annual ebullitive CH₄ fluxes were significantly higher in the Silex pond than the
 605 Tenreuken pond (Tukey's HSD test p<0.0001) that showed a higher macrophyte cover during summer (100% in the Silex
 606 pond and 68% in the Tenreuken pond) and were not significantly different in the two turbid-water Leybeek and Pêcherries
 607 ponds (Tukey's HSD test p=0.3847) that showed similar macrophyte cover during summer (6 and 9% in the Leybeek and
 608 Pêcherries ponds, respectively) (Fig. 8). The annual ebullitive CH₄ fluxes were overall positively correlated to macrophyte
 609 cover and negatively correlated to Chl-*a* (Fig. 8). The higher ebullitive CH₄ emissions from the clear-water ponds (~~Leybeek
 610 and Pêcherries~~) and were positively correlated to macrophyte cover and negatively related to Chl-*a* (Fig. 8). This would
 611 suggest that the delivery of organic matter to sediments from macrophytes sustained a larger methane production than from
 612 phytoplankton. This finding is consistent with the notion that vegetated littoral zones of lakes are hot spots of CH₄
 613 production and emission (e.g. Hyvönen et al., 1998; Huttunen et al., 2003; Juutinen et al., 2003; Desrosiers et al., 2022). In
 614 other small lentic systems, the CH₄ dissolved concentrations and diffusive fluxes have also been shown to correlate
 615 positively with macrophyte cover (e.g. Ray et al., 2023; Theus et al., 2023).

616 The annual diffusive CH₄ flux was higher in the two clear-water ~~lakes~~ ponds (1.4±0.7 and 1.9±0.4 mmol m⁻² d⁻¹ in the
 617 ~~Tenreuken and Silex~~ ponds, respectively) (~~Tenreuken and Silex~~) than in ~~one of~~ the turbid-water ~~lakes~~ (Pêcherries) pond
 618 (1.0±0.3 mmol m⁻² d⁻¹) (Tukey's HSD test p=0.0404 for Tenreuken versus Pêcherries, and p<0.0001 for Silex versus
 619 Pêcherries), which ~~is was~~ consistent with the pattern of higher ebullitive CH₄ emissions from clear-water ~~lakes~~ ponds (Fig. 8).
 620 In the four sampled urban ponds, annual CH₄ diffusive fluxes were significantly higher in the pond with the highest total

621 macrophyte cover in the clear-water ponds, and significantly higher in the pond with highest Chl-*a* concentration in the
 622 turbid-water ponds ~~increased in clear water ponds with increasing total macrophyte cover and in turbid water ponds with~~
 623 ~~increasing Chl-*a*~~ (Fig. 8). An increase in methane production with phytoplankton biomass in turbid-water ponds has also
 624 been reported by other studies in lakes ~~This suggests that in turbid water lakes the methane production increases with~~
 625 ~~phytoplankton biomass, as suggested in other studies~~ (e.g. Yan et al., 2019; Bartosiewicz et al., 2021; ~~Borges et al., 2022~~).
 626 Since total macrophyte cover and Chl-*a* were anti-correlated, we hypothesize that the variations of CH₄ diffusive fluxes
 627 follow a U-shaped relation with either Chl-*a* or macrophyte cover. Higher values of annual CH₄ diffusive fluxes occurred at
 628 the extreme values of Chl-*a* or ~~of~~ macrophyte cover (minimum or maximum), and lower values occurred at the intermediate
 629 values of Chl-*a* or macrophyte cover. The relative contribution of ebullitive CH₄ fluxes to the total flux ~~was higher in the~~
 630 ~~clear-water Silex pond, which had the highest macrophyte cover, compared to the two turbid-water ponds with lower~~
 631 ~~macrophyte cover (Tukey's HSD test p<0.0001 for Silex versus Leybeek, p=0.0056 for Silex versus Pêcheres), and was~~
 632 ~~higher in the clear-water Tenreuken pond than in the turbid-water Leybeek pond (Tukey's HSD test p<0.0001) (Fig. 8). The~~
 633 ~~relative contribution of ebullitive CH₄ fluxes to the total CH₄ flux seems to increase concomitantly with the macrophyte~~
 634 ~~cover (Fig. 8), and was overall very strongly positively correlated positively~~ to macrophyte cover and negatively to Chl-*a*
 635 (Fig. 8). ~~These is patterns is~~ are consistent with the idea of an increase of ebullition relative to diffusive CH₄ emissions in
 636 vegetated sediments compared to unvegetated sediments (e.g. Desrosiers et al., 2022; Ray et al., 2023; Theus et al., 2023).

637 The annual diffusive and ebullitive fluxes in the four ponds in the city of Brussels were within the range of values for ponds
 638 of similar surface area (0.4 to 4.0 ha) compiled by Deemer and Holgerson (2021) (Fig. S11~~5~~). The linear regression of
 639 ebullitive CH₄ fluxes as a function of diffusive CH₄ fluxes allows comparing the data of ebullitive CH₄ fluxes from the ~~four~~
 640 Brussels ponds “normalized” to the diffusive CH₄ fluxes. The ebullitive CH₄ fluxes from the two turbid-water ponds
 641 (Pêcheres and Leybeek) were very close to the linear regression showing they were characterized by ebullitive CH₄ fluxes
 642 equivalent to those in the ponds compiled by Deemer and Holgerson (2021) when normalized by the diffusive fluxes. The
 643 ebullitive CH₄ fluxes from the two clear-water ponds (Tenreuken and Silex) were above the linear regression showing they
 644 were characterized by ebullitive CH₄ fluxes above those in the ponds compiled by Deemer and Holgerson (2021) when
 645 normalized by the diffusive fluxes. We hypothesize the relatively higher ebullitive fluxes in the two clear-water ponds were
 646 related to enhancement of ebullition from ~~organic matter subsidized by~~ macrophytes. This ~~hypothesis~~ is consistent with the
 647 two clear-water ponds in Brussels having ~~higher~~ ebullitive fluxes ~~higher~~ than in the ponds compiled by Deemer and
 648 Holgerson (2021) at equivalent Chl-*a* values (Fig. S11). ~~The is observed high ebullitive fluxes in the clear-water ponds~~ would
 649 suggest that Chl-*a* concentration alone fails to predict ebullitive fluxes in macrophyte-dominated clear-water ponds.
 650 Consequently, global scaling of CH₄ fluxes in ~~lakes-lentic systems~~ using Chl-*a* as a predictor ~~as used in lakes~~ (e.g. DelSontro
 651 et al., 2018) might under-estimate ebullitive CH₄ emissions due to a misrepresentation of macrophyte-dominated clear-water
 652 ponds.

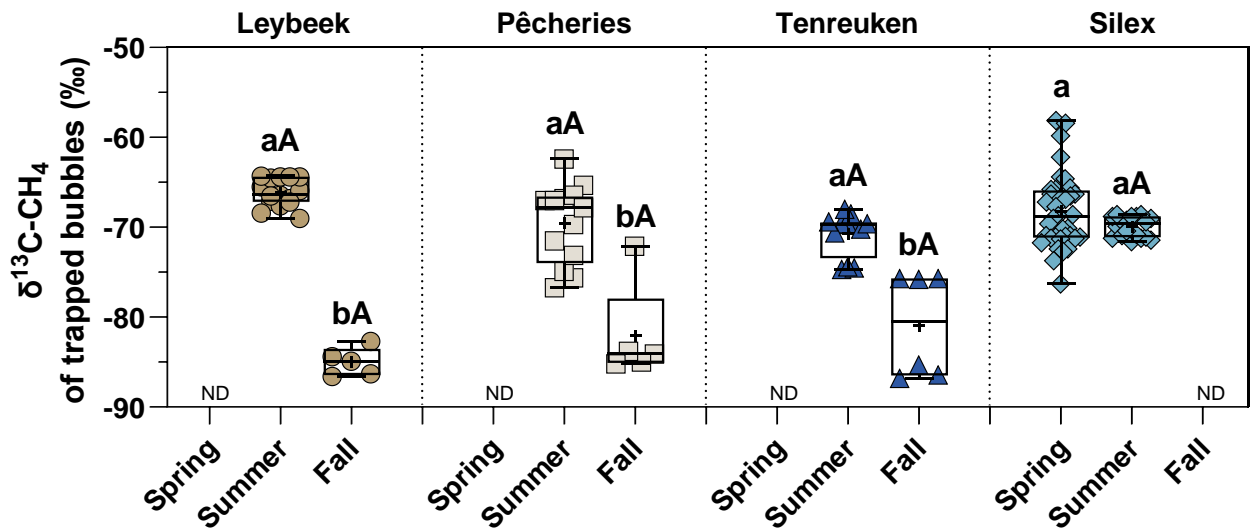
653 The annual averaged diffusive fluxes of CO₂ (F_{CO2}) and N₂O (F_{N2O}) in the four ponds in the city of Brussels were also plotted
 654 against Chl-*a* concentration, total macrophyte cover in summer, water depth, and lake surface area, as well as DIN for N₂O
 655 fluxes (Figs. S12, S13, S14). Annual F_{CO2} did not show significant differences between the four studied ponds (Tukey's HSD
 656 test: p>0.05 for each comparison), and F_{CO2} did not significantly correlate to the other variables (Chl-*a* concentration, total
 657 macrophyte cover, water depth, and lake surface area). This might be surprising since other studies have reported lower CO₂
 658 fluxes in more productive lentic systems (e.g. Sand-Jensen and Staehr 2007; Borges et al. 2022). We hypothesize that given
 659 that the four systems were either phytoplankton-dominated or macrophyte-dominated, in both cases, the ponds had an
 660 important submerged productivity resulting in a relatively invariant F_{CO2} as function of either Chl-*a* or macrophyte cover.

Annual mean F_{CO_2} was also uncorrelated to water depth and lake area (Fig. S12). This might have resulted from the relative similarity of depth and surface area of the four studied ponds, as it is well established that CO_2 emissions strongly increase with decreasing size of ponds (Holgerson and Raymond, 2016). Annual F_{N_2O} was not significantly different between clear-water and turbid-water ponds. F_{N_2O} was significantly lower in the slightly deeper Pêcheries pond than the two slightly shallower Leybeek and Silex ponds (Fig. S13) (Tukey's HSD test $p=0.0012$ for Pêcheries vs. Leybeek, and $p=0.0052$ for Pêcheries vs. Silex), and F_{N_2O} showed a significant negative relationship with water depth (Fig. S13). We hypothesize that this might reflect a larger dilution of N_2O diffusing from sediments in the deeper systems. F_{N_2O} did not correlate to DIN, NH_4^+ , NO_2^- , and NO_3^- (Fig. S14). We hypothesize that this reflects the rather narrow range of annual DIN average values in the four studied ponds (~ 24 to $\sim 29 \mu mol L^{-1}$), as DIN, NH_4^+ , NO_2^- , and NO_3^- were not statistically different between ponds (Tukey's HSD test $p>0.05$ for every comparison).

3.5. Methanogenesis pathway inferred from $\delta^{13}C-CH_4$ in bubbles

$\delta^{13}C-CH_4$ was measured in bubbles trapped during the ebullition flux measurements and in bubbles collected by perturbing the sediments. The variations of $\delta^{13}C-CH_4$ suggest that there could have been variations of the relative importance of hydrogenotrophic versus acetoclastic pathways of methanogenesis among different ponds but also seasonally. Methanogenesis by the hydrogenotrophic pathway produces CH_4 with more negative $\delta^{13}C-CH_4$ values (-100‰ to -60‰) compared to the acetoclastic pathway (-65‰ to -50‰) (Whiticar et al., 1986). Yet, it remains unclear which environmental factors determine the relative importance of hydrogenotrophic and acetoclastic methanogenesis pathways (Conrad et al., 2011).

The $\delta^{13}C-CH_4$ values in the trapped bubbles for the all dataset wereas statistically more negative in fall ($-83.2\pm 5.2 \text{‰}$) than summer ($-69.5\pm 3.2 \text{‰}$) and spring ($-68.2\pm 4.4 \text{‰}$) (Fig. 9; Table S8) (Tukey's HSD test $p<0.0001$ for fall versus summer, and fall versus spring), suggesting a dominance of hydrogenotrophic methanogenesis in fall compared to spring and summer when acetoclastic methanogenesis seemed dominant. Hydrogenotrophic methanogenesis occurs at higher temperatures than acetoclastic methanogenesis (Schulz and Conrad, 1996; Schulz et al., 1997), however, temperature in fall ($11.9\pm 3.7 \text{ °C}$) was lower than in summer ($21.1\pm 1.9 \text{ °C}$) (Tukey's HSD test $p<0.0001$). A shift from acetoclastic methanogenesis to hydrogenotrophic methanogenesis has been documented in response to the increase of NH_4^+ concentration (Ni et al., 2022; Wang et al., 2022) and the decrease of pH (Kotsyurbenko et al., 2007) expected in response to an increase of CO_2 . An increase of NH_4^+ and decrease of pH in pore waters in fall compared to summer and spring would be consistent with the sustained benthic organic matter degradation leading to a gradual change of pore water chemistry from spring to fall.



690

691 | **Figure 9:** $\delta^{13}\text{C}/^{12}\text{C}$ ratio of CH_4 ($\delta^{13}\text{C}-\text{CH}_4$, in ‰) in bubbles collected during ebullitive flux measurements (“trapped bubbles”) in
692 | four urban ponds (Leybeek, Pêcherries, Tenreuken, and Silex) in the city of Brussels (Belgium), measured in spring, summer, and
693 | fall in 2022 and 2023 (September 2023 and October 2023 in the Leybeek pond; July 2023 and October 2023 in the Pêcherries pond;
694 | August 2023 and October 2023 in the Tenreuken pond; April 2022 and July 2022 in the Silex pond). Box plots show median
695 | (horizontal line), mean (cross), and 25–75% percentiles (box limits). Whiskers extend from minimum to maximum values. ND = no
696 | data. ANOVA results of the multiple comparison between boxplots are summarized in Table S7. ANOVA results of the multiple
697 | comparison between boxplots are summarized in Table S8. Different lower-case letters indicate significant differences between
698 | seasons for a given pond and upper-case letters indicate significant differences between ponds within a season.

699 | In summer 2023, a survey of all four ponds was made to simultaneously sample bubbles by perturbation of the sediment for
700 | the determination of the $\delta^{13}\text{C}-\text{CH}_4$ in the released bubbles. The $\delta^{13}\text{C}-\text{CH}_4$ values of perturbed sediments was were more
701 | negative in the clear-water macrophyte-dominated ponds (-80.1 ± 0.1 ‰ and -78.4 ± 1.2 ‰ in the Tenreuken and Silex ponds,
702 | respectively) than in the turbid-water phytoplankton-dominated ponds (-69.7 ± 0.7 ‰ and -70.7 ± 0.4 ‰ in the Leybeek and Pêcherries ponds, respectively) (Tukey’s HSD test $p < 0.0001$ for each comparison between a clear
703 | pond and a turbid pond) (Fig. 10). This pattern of $\delta^{13}\text{C}-\text{CH}_4$ of perturbed sediments could suggest a higher contribution of the
704 | hydrogenotrophic methanogenesis pathway compared to the acetoclastic pathway in the clear-water ponds where organic
705 | matter for methanogenesis was assumed to be mainly related to macrophytes rather than phytoplankton. Based on gene
706 | expression during incubations (qPCR), Wang et al., (2023) suggested that acetoclastic methanogenesis pathway was
707 | stimulated by macrophyte organic carbon stimulated acetoclastic methanogenesis pathway compared to phytoplankton
708 | organic matter in lakes Chaohu and Taihu in China. The pattern-distribution of $\delta^{13}\text{C}-\text{CH}_4$ data in the four urban ponds of the
709 | city of Brussels suggests the opposite pattern, with macrophyte organic carbon stimulating the hydrogenotrophic
710 | methanogenesis pathway. This pattern seems consistent with the more refractory nature of macrophyte organic carbon
711 | compared to the more labile nature of phytoplankton organic carbon. Organic matter from macrophytes has a large share of
712 | molecules difficult to degrade such as cellulose unlike organic matter from phytoplankton that is rich in polysaccharides and
713 | proteins (West et al., 2015; Berberich et al., 2020). In presence of more refractory organic matter, a partial fermentation
714 | would favour the production of H_2 over acetate which would favour hydrogenotrophic methanogenesis over acetoclastic
715 | methanogenesis (Liu et al., 2017).

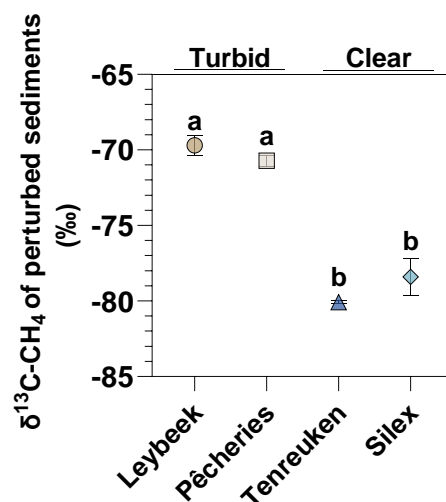


Figure 10: Mean \pm standard deviation $^{132}\text{C}/^{123}\text{C}$ ratio of CH_4 ($\delta^{13}\text{C-CH}_4$, in ‰) in bubbles sampled after released from sediments after physical perturbation (“perturbed sediments”) versus chlorophyll a ($\text{Chl } a$, in $\mu\text{g L}^{-1}$) and total macrophyte cover in summer (%) in four ponds (Leybeek, Pêcherries, Tenreuken, and Silex) in the city of Brussels (Belgium) measured in summer 2023 (4th September 2023). Error bars indicate standard deviation on the mean. Dashed lines indicate linear regressions (Table S5). ANOVA results of the multiple comparison between boxplots are summarized in Table S9. Different lower-case letters indicate significant differences between ponds.

3.6. Methane oxidation

The $\delta^{13}\text{C-CH}_4$ of dissolved CH_4 in surface waters in the four sampled ponds in the city of Brussels ranged between -16 and -64 ‰ (Fig. 11). The $\delta^{13}\text{C-CH}_4$ of dissolved CH_4 in surface waters were generally higher than in sediments based on trapped bubbles during the ebullition measurements (-55 to -87 ‰; Fig. 9). The ^{13}C enriched values of dissolved CH_4 in surface waters samples probably resulted from MOX. FOX in surface waters in the four sampled ponds in the city of Brussels ranged between 22 and 97%. MOX in surface waters in the four sampled ponds in the city of Brussels ranged between 0.1 and 73.0 $\text{mmol m}^{-2} \text{d}^{-1}$ (Fig. 11).

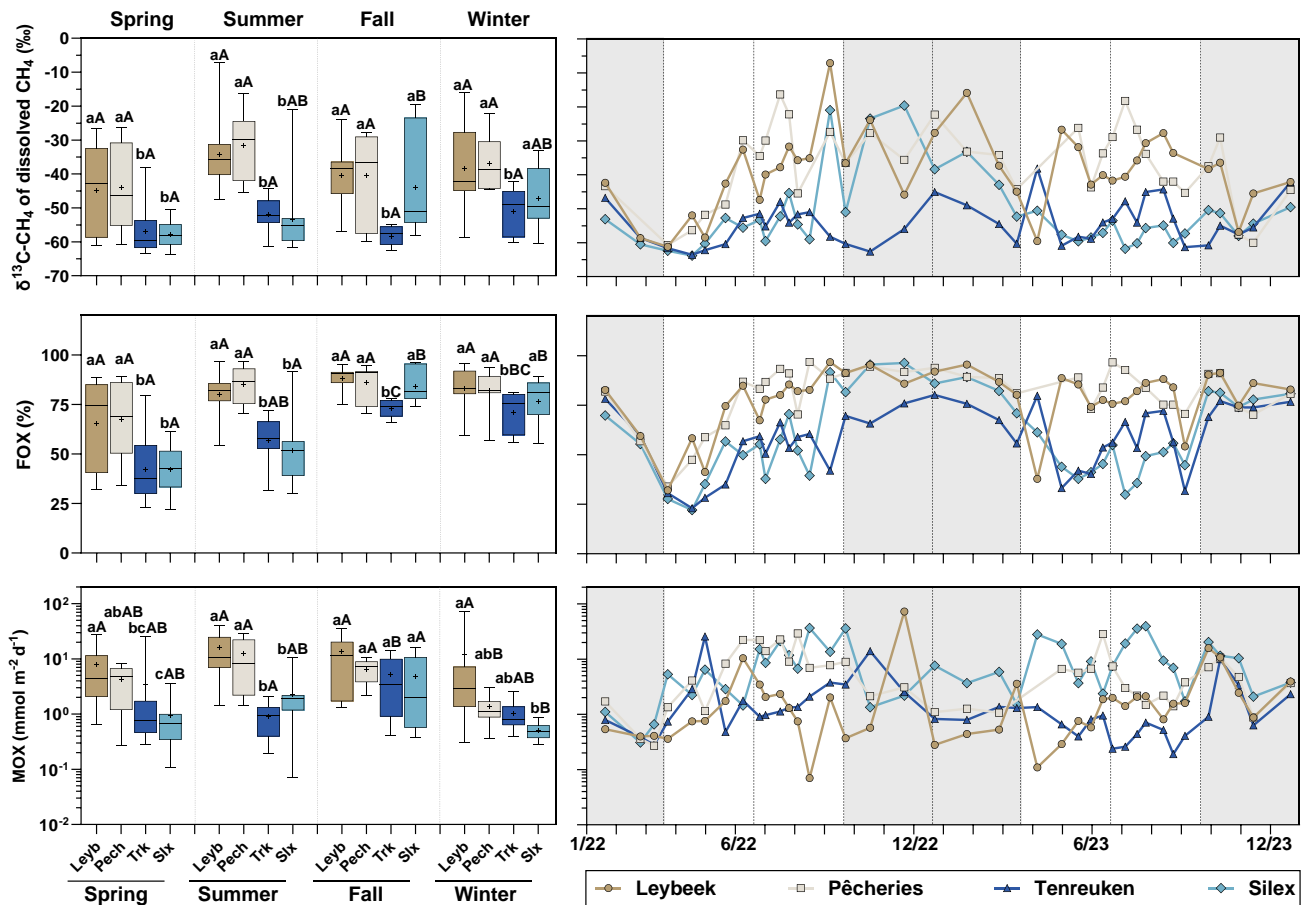


Figure 11: Seasonal variations of $\delta^{13}\text{C}/^{12}\text{C}$ ratio of dissolved CH_4 in surface waters ($\delta^{13}\text{C}\text{-CH}_4$ of dissolved CH_4 , in ‰), fraction of CH_4 removed by methane oxidation (FOX, in %), and methane oxidation (MOX, in $\text{mmol m}^{-2} \text{d}^{-1}$) in four urban ponds (Leybeek (Leyb), Pêcherries (Pech), Tenreuken (Trk), and Silex (Slx)) in the city of Brussels (Belgium) from January 2022 to December 2023. Box plots show median (horizontal line), mean (cross), and 25–75% percentiles (box limits). Whiskers extend from minimum to maximum values. White and grey bands in the graphs on the right correspond to the fall/winter and spring/summer periods, and dotted vertical bars represent the first days of each season. ANOVA results of the multiple comparison between boxplots are summarized in Tables S4 and S5. Different lower-case letters indicate significant differences between ponds within a season and different upper-case letters indicate significant differences between seasons for a given pond. ANOVA results of the multiple comparison between boxplots are summarized in Table S6.

FOX and MOX followed the same seasonal variations than $\delta^{13}\text{C}\text{-CH}_4$ of dissolved CH_4 since both quantities were derived from isotopic models that include $\delta^{13}\text{C}\text{-CH}_4$ of dissolved CH_4 . $\delta^{13}\text{C}\text{-CH}_4$ of dissolved CH_4 , FOX, and MOX showed no significant differences between seasons in the two turbid-water ponds except in the Pêcherries pond where MOX was lower in winter ($1.3 \pm 0.86 \text{ mmol m}^{-2} \text{d}^{-1}$) than in summer ($12.3 \pm 10.5 \text{ mmol m}^{-2} \text{d}^{-1}$, Tukey's HSD test $p=0.0010$) and fall ($6.5 \pm 3.0 \text{ mmol m}^{-2} \text{d}^{-1}$, Tukey's HSD test $p=0.0254$) (Fig. 11). In the clear-water Silex pond, FOX was lower in spring ($42 \pm 12 \%$) and summer ($52 \pm 16 \%$) than in fall ($84 \pm 9 \%$) and winter ($76 \pm 12 \%$) (Tukey's HSD test $p < 0.0001$ for spring or summer versus fall or winter). In the clear-water Tenreuken pond, FOX was higher in fall ($73 \pm 5 \%$) than in spring ($42 \pm 17 \%$, Tukey's HSD test $p < 0.0001$) and summer ($57 \pm 11 \%$, Tukey's HSD test $p=0.0324$), and higher in winter ($71 \pm 10 \%$) than in spring ($42 \pm 17 \%$, Tukey's HSD test $p < 0.0001$) were in most ponds higher in summer and fall than in spring and winter (Fig. 11). $\delta^{13}\text{C}\text{-CH}_4$, FOX, and MOX showed distinct differences among the four ponds. $\delta^{13}\text{C}\text{-CH}_4$ of dissolved CH_4 and FOX, and MOX were statistically higher in the turbid-water ponds (Leybeek and Pêcherries) than in the clear-water ponds (Tenreuken and Silex), particularly during spring and summer (Fig. 11) and than in the Tenreuken pond during fall and winter (Fig. 11; Tables S4 and S5). These seasonal differences led to an annual MOX that was statistically higher in the turbid-water ponds (10.8 and $7.2 \text{ mmol m}^{-2} \text{d}^{-1}$ in the Leybeek and Pêcherries ponds, respectively) than the clear-water ponds (2.4 and $4.4 \text{ mmol m}^{-2} \text{d}^{-1}$ in the Tenreuken and Silex ponds, respectively) (Tukey's HSD test $p < 0.0001$ for each turbid-water pond versus each clear-

water pond). TSM and Chl-*a* concentrations were higher in the turbid-water ponds than in the clear-water ponds, particularly during productive phytoplanktonic periods of spring and summer (Fig. 3), when the highest difference of $\delta^{13}\text{C}\text{-CH}_4$ of dissolved CH_4 , FOX, and MOX were observed between the turbid-water and the clear-water ponds (Fig. 11).

$\delta^{13}\text{C}\text{-CH}_4$ of dissolved CH_4 , FOX, and MOX positively correlated to TSM and Chl-*a* concentrations (Fig. 12). These patterns could reflect the increase of micro-organisms including methanotrophs fixed on particles leading to an increase of MOX in parallel to an increase of TSM concentration (Abril et al., 2007). Fixed micro-organisms can grow on fixed inorganic particles and, aggregates of organic matter (Kirchman and Mitchell, 1982), but also on aggregates of living cyanobacteria (Li et al., 2021). An increase of particles in the water column increases light attenuation in the water column which would alleviate the inhibition of MOX by light (Dumestre et al., 1999; Murase and Sugimoto 2005; Morana et al., 2020), also possibly contributing to a positive relation between MOX and TSM and Chl-*a*, along the turbidity gradient. Both processes could co-occur contributing to the observed positive patterns between MOX and TSM and Chl-*a* concentrations.

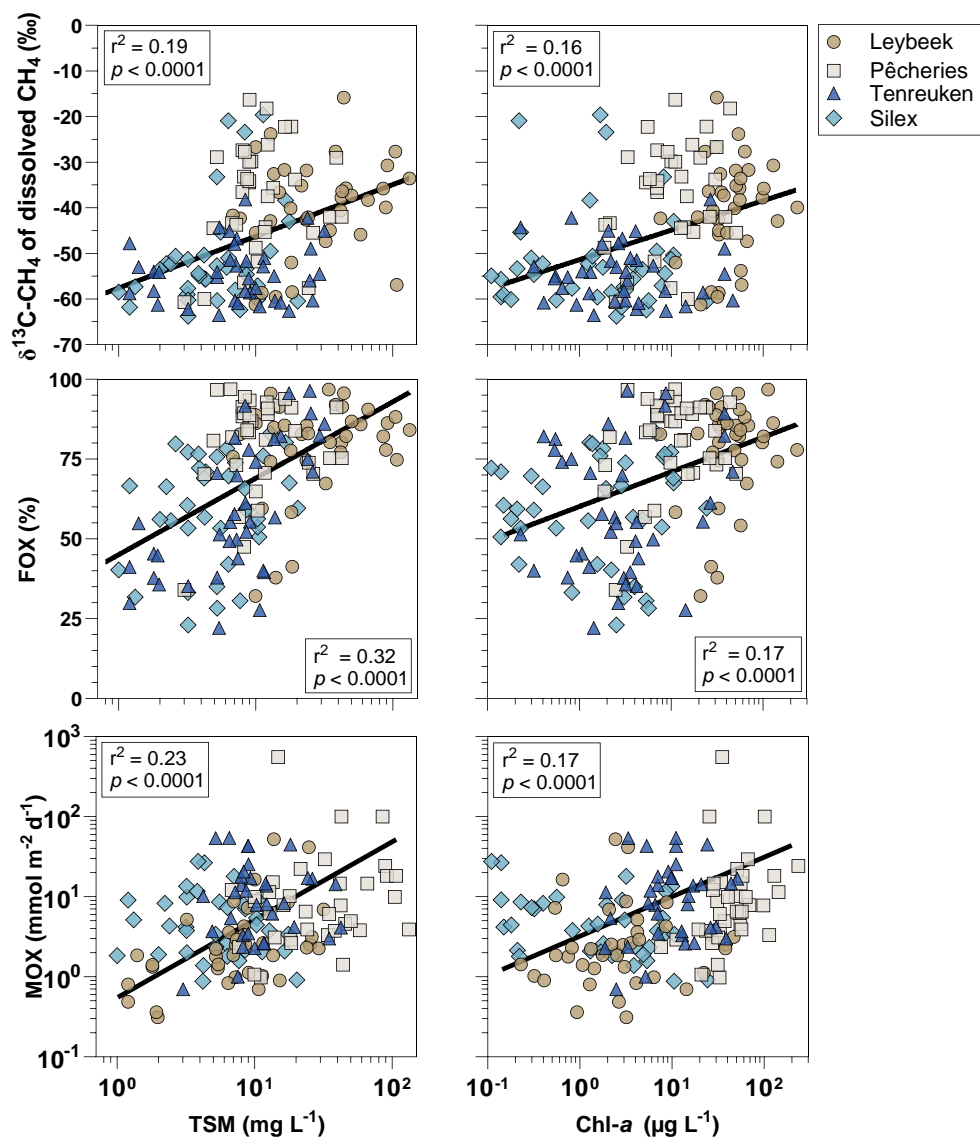


Figure 12: $^{12}\text{C}/^{13}\text{C}$ ratio of CH_4 in surface waters ($\delta^{13}\text{C}\text{-CH}_4$, in ‰), fraction of CH_4 removed by methane oxidation (FOX, in %), and methane oxidation flux (MOX, in $\text{mmol m}^{-2} \text{d}^{-1}$) versus total suspended matter concentration (TSM, in mg L^{-1}) and chlorophyll-*a*

concentration ($\text{Chl-}a$, in $\mu\text{g L}^{-1}$) in four urban ponds (Leybeek, Pêcherries, Tenreuken, and Silex) in the city of Brussels (Belgium) from January 2022 to December 2023. Linear regression shown as black solid line (Table S115).

Figure S153 compares the main fluxes of dissolved CH_4 in the water column: MOX, diffusive CH_4 emissions, bubble dissolution that were derived from measurements, and the sedimentary diffusive CH_4 flux that was computed as a closing term (assuming a steady state) for comparative purposes. The dissolution of bubbles was a significantly smaller input term of dissolved CH_4 compared to the diffusive sedimentary flux that represented 88 ± 18 % of the total input of CH_4 to the water column (Tukey's HSD test $p < 0.0001$ in each pond). The low contribution of dissolution of bubbles resulted from the shallowness of the studied ponds because bubble dissolution depends on the time spent by the bubble in the water column during ascent, which is directly proportional to depth (McGinnis et al., 2006). MOX was a larger sink of dissolved CH_4 than the diffusive CH_4 emission to the atmosphere in the four ponds, representing 80 ± 19 % and 80 ± 14 % of the total dissolved CH_4 removal in the turbid-water Leybeek and Pêcherries ponds respectively (Tukey's HSD test $p < 0.0001$ for the two ponds), and 59 ± 21 % and 51 ± 27 % in the clear-water Tenreuken and Silex ponds respectively (Tukey's HSD test $p = 0.3429$ for the Tenreuken pond, and $p = 0.7634$ for the Silex pond). For all four ponds, MOX accounted for 6678 ± 26 % of the total CH_4 dissolved removal from the water column, in agreement with other studies in lentic systems (Kankaala et al., 2006; Bastviken et al., 2008; Morana et al., 2020; Reis et al., 2022).

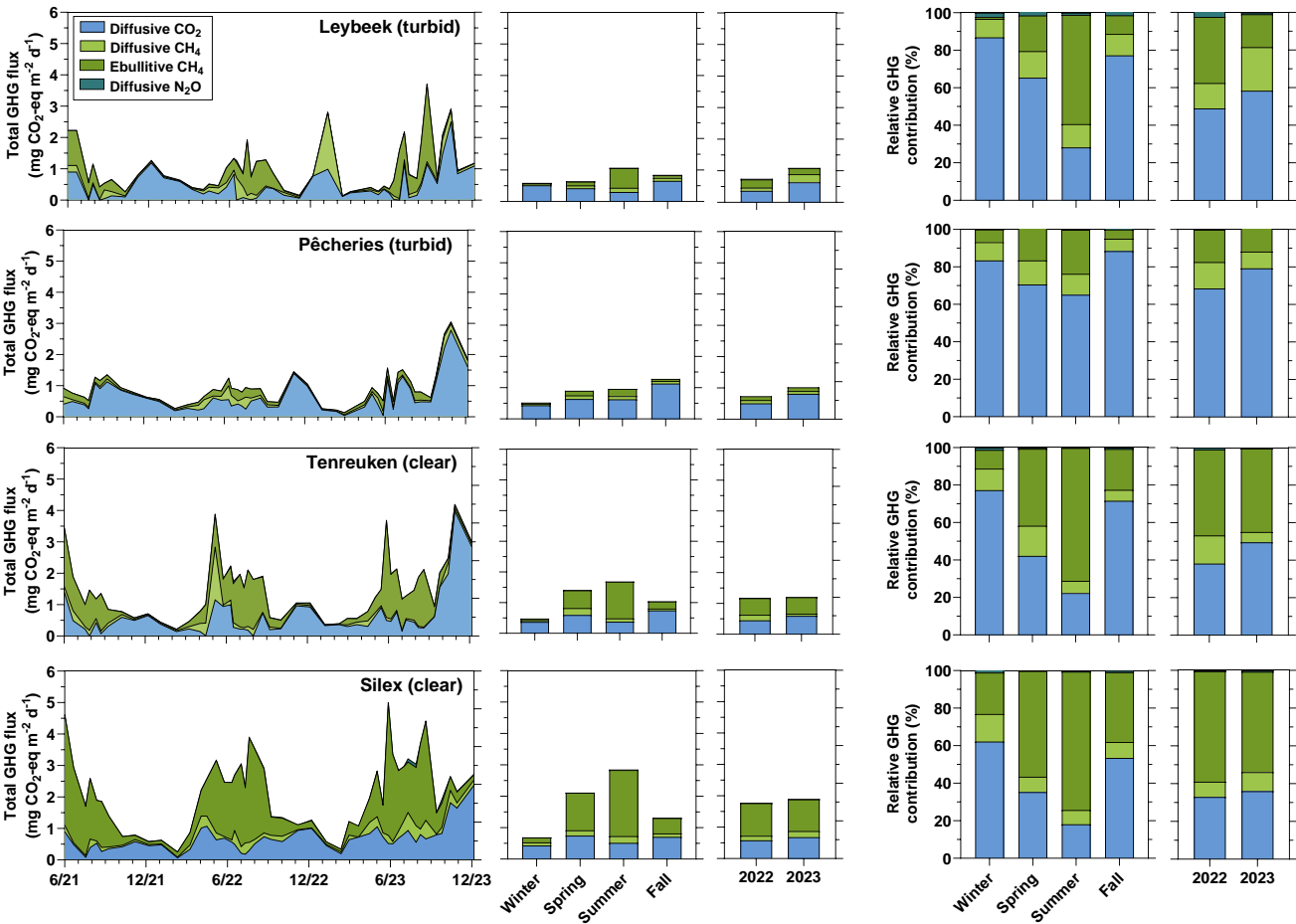
3.7. Relative contribution of CO_2 , CH_4 and N_2O emissions

The emissions in CO_2 -eq for the 3 GHGs averaged per season for both 2022 and 2023 peaked seasonally in summer with 2.9 and 1.7 $\text{mg CO}_2\text{-eq m}^{-2} \text{d}^{-1}$ in the Silex and the Tenreuken ponds, respectively, and 1.1 $\text{mg CO}_2\text{-eq m}^{-2} \text{d}^{-1}$ in the Leybeek pond (Fig. 13). The GHG fluxes peaked in fall in the Pêcherries pond, with 1.3 $\text{mg CO}_2\text{-eq m}^{-2} \text{d}^{-1}$. The higher value of the total GHG emissions in fall compared to other seasons in the Pêcherries pond was due to an increase of CO_2 emissions in fall that surpassed the peak of CH_4 emissions in summer. The GHG fluxes were the lowest in winter with 1.3 and 0.9 $\text{mg CO}_2\text{-eq m}^{-2} \text{d}^{-1}$ in the Silex and the Tenreuken ponds, respectively, and 0.8 and 0.6 $\text{mg CO}_2\text{-eq m}^{-2} \text{d}^{-1}$ in the Pêcherries and the Leybeek ponds, respectively. The relative contribution of ebullitive CH_4 fluxes peaked in summer in all four ponds, 73.8% and 70.9% in the Silex and the Tenreuken ponds, respectively, and 23.6% and 58.3% in the Pêcherries and the Leybeek ponds, respectively. The relative contribution of ebullitive CH_4 fluxes was lowest in winter with 22.1% and 10.0% in the Silex and the Tenreuken ponds, respectively, and 6.7% and 1.0% in the Pêcherries and the Leybeek ponds, respectively.

The annual fluxes-emissions in CO_2 -eq of the three GHGs (CO_2 , CH_4 , and N_2O) in 2022 and 2023 were higher in the two clear-water ponds (1.3 ± 0.5 and 1.8 ± 0.9 $\text{mg CO}_2\text{-eq m}^{-2} \text{d}^{-1}$ in the Tenreuken and Silex ponds, respectively) than in the two turbid-water ponds (1.0 ± 0.2 and 0.9 ± 0.5 $\text{mg CO}_2\text{-eq m}^{-2} \text{d}^{-1}$ in the Leybeek and Pêcherries ponds, respectively) (Fig. 134) (Tukey's HSD test $p < 0.0001$ for Silex versus Pêcherries, $p < 0.0001$ for Silex versus Leybeek, $p = 0.0107$ for Tenreuken versus Pêcherries, and $p = 0.0467$ for Tenreuken versus Leybeek) due to higher total CH_4 emissions (diffusive+ebullitive) in clear-water ponds (0.7 ± 0.4 and 1.2 ± 0.5 $\text{mg CO}_2\text{-eq m}^{-2} \text{d}^{-1}$ in the Tenreuken and Silex ponds, respectively) than in turbid-water ponds (0.2 ± 0.2 and 0.4 ± 0.3 $\text{mg CO}_2\text{-eq m}^{-2} \text{d}^{-1}$ in the Leybeek and Pêcherries ponds, respectively) (Tukey's HSD test $p < 0.0001$ for Silex versus Pêcherries, $p < 0.0001$ for Silex versus Leybeek, $p = 0.0005$ for Tenreuken versus Pêcherries, and $p = 0.0164$ for Tenreuken versus Leybeek), as there were no significant differences between the four ponds for CO_2 and N_2O emissions in 2022 and 2023 (Tukey's HSD test $p > 0.05$ for each comparison). N_2O emissions were significantly lower in the Pêcherries pond than the Leybeek and Silex ponds (Tukey's HSD test $p = 0.0012$ for Pêcherries versus Leybeek, and $p = 0.0052$ for Pêcherries versus Silex). The contribution of N_2O to the total GHG emissions was marginal and did not affect the differences in total GHG fluxes between ponds, with the highest contribution observed in the Leybeek pond, with a contribution of 1.7%.

811 The majority of GHG emissions in CO₂-eq was related to CO₂ and CH₄ (diffusive+ebullitive) in the four ponds. In turbid-
 812 water ponds CO₂ represented the largest fraction of GHG emissions (68.5% (2022) and 79.3% (2023) in the Pêcheries pond,
 813 and 49.0% (2022) and 58.3% (2023) in the Pêcheries and Leybeek ponds, respectively). , and In clear-water ponds CH₄
 814 represented the largest fraction of GHG emissions (66.5% (2022) and 63.3% (2023) in the Silex pond, and 60.8% (2022) and
 815 50.0% (2023), in the Silex and Tenreuken ponds, respectively). The higher annual GHG emissions in CO₂-eq from the two
 816 clear-water ponds than the turbid-water ponds were related to the higher contribution of ebullitive CH₄ fluxes. N₂O
 817 contribution to GHG emissions was marginal and ranged between 0.0% in the Pêcheries pond that occasionally acts as a sink
 818 and 1.7% in the Leybeek pond.

819 The GHG fluxes peaked seasonally in summer with 2.9 and 1.7 mg CO₂-eq m⁻² d⁻¹ in the Silex and the Tenreuken ponds,
 820 respectively, and 1.1 mg CO₂-eq m⁻² d⁻¹ in the Leybeek pond. The GHG fluxes peaked in fall in the Pêcheries, with 1.3 mg
 821 CO₂-eq m⁻² d⁻¹. The higher value of the total GHG emissions in fall compared to other seasons in the Pêcheries pond is due
 822 to the summer increase in CH₄ was lower than the CO₂ increase in fall, which particularly increased in fall 2023. The GHG
 823 fluxes were the lowest in winter with 1.3 and 0.9 mg CO₂-eq m⁻² d⁻¹ in the Silex and the Tenreuken ponds, respectively, and
 824 0.8 and 0.6 mg CO₂-eq m⁻² d⁻¹ in the Pêcheries and the Leybeek ponds, respectively. The relative contribution of ebullitive
 825 CH₄ fluxes peaked in summer in all four ponds, 73.8% and 70.9% in the Silex and the Tenreuken ponds, respectively, and
 826 23.6% and 58.3% in the Pêcheries and the Leybeek ponds, respectively. The relative contribution of ebullitive CH₄ fluxes
 827 was lowest in winter with 22.1% and 10.0% in the Silex and the Tenreuken ponds, respectively, and 6.7% and 1.0% in the
 828 Pêcheries and the Leybeek ponds, respectively.



829

830 | **Figure 134: Temporal evolution and relative contribution of emissions to the atmosphere of CO₂ (diffusive), CH₄ (diffusive and**
 831 **ebullitive), and N₂O (diffusive) expressed in CO₂ equivalents (in mg CO₂-eq m⁻² d⁻¹), in four urban ponds (Leybeek, Pêcheres,**
 832 **Tenreuken, and Silex) in the city of Brussels (Belgium) from June 2021 to December 2023. Averages per season include data from**
 833 **2021, 2022, and 2023. Year 2023 had a higher annual precipitation (1011 mm) than year 2022 (701 mm).**

834 The annual GHG fluxes increased from 2022 to 2023 due to an increase in relative contribution of CO₂ diffusive emissions
 835 in all four ponds. Diffusive CO₂ ~~diffusive~~-emissions averaged annually in all four ponds 0.5 mg CO₂ m⁻² d⁻¹ in 2022 and 0.7
 836 mg CO₂ m⁻² d⁻¹ in 2023. Diffusive CO₂ emissions were two times higher in summer 2023 than in summer 2022, and 2.5
 837 times higher in fall 2023 than in fall 2022, for similar values between 2023 and 2022 in spring and winter (1.1 higher and 1.1
 838 lower, respectively). Air temperatures were similar in both years (annual average of 12.2°C in 2022 and 12.1°C in 2023)
 839 with winter, spring and summer marginally colder in 2023 than in 2022 (-0.5, -1.1°C and -0.4°C, respectively), and fall
 840 marginally warmer in 2023 than 2022 (+0.6°C). Spring and summer ~~and fall~~ were rainier in 2023 than 2022 (2.2 and -2.5
 841 and 1.4-times, respectively) ~~and but fall and winter precipitations were relatively similar in both years (1.4 times wetter and~~
 842 ~~2023 was 1.2 times drier in 2023 than winter 2022, respectively). Winter, spring and summer were colder in 2023 than in~~
 843 ~~2022 (-0.5, -1.1°C and -0.4°C, respectively), and fall was warmer in 2023 than 2022 (+0.6°C).~~ Higher precipitations are
 844 likely to increase the inputs of organic and inorganic carbon from soils to ponds by ground-waters, soil-waters, and surface
 845 runoff, as previously shown in other ~~lakes-lentic systems~~ (e.g. Marotta et al., 2011; Holgerson, 2015). ~~Higher runoff~~
 846 ~~combined with higher temperature led to more favourable conditions for OM degradation and respiration.~~ The highest
 847 seasonal increase of diffusive CO₂ emissions was observed in fall 2023. ~~(rainier and warmer in 2023 than in 2022), followed~~
 848 ~~by summer and spring, which showed the higher decrease of temperature in 2023 compared to 2022.~~ While this hypothesis is
 849 only based on the comparison of two years, the increase of the relative contribution of CO₂ diffusive emissions was observed
 850 in all four ponds which suggests a common uniform driver that would be consistent with a large variation weather such as
 851 annual precipitation. The El Niño event in 2023 ~~has~~ induced low-level cyclonic wind anomalies and higher precipitation over
 852 Western Europe, including Belgium (Chen et al., 2024).

853 4. Conclusions

854 We found very marked differences in CH₄ dynamics between the two clear-water macrophyte-dominated ponds (Tenreuken
 855 and Silex) and the two turbid-water ~~phytoplankton-dominated~~phytoplankton-dominated ponds (Pêcheres and Leybeek) of
 856 the city of Brussels. MOX was more important in the two turbid-water ponds compared to the clear-water ponds. MOX
 857 correlated to TSM and Chl-*a* concentrations possibly owing to a higher abundance of methanotrophs in the water column
 858 fixed to particles and/or an attenuation of light limitation of MOX. Ebullitive CH₄ emissions were higher in the two clear-
 859 water ponds than the two turbid-water ponds, possibly related to high availability of macrophyte organic matter. The annual
 860 diffusive N₂O and CO₂ fluxes in 2022-2023 were not statistically different in the two clear-water ponds (Tenreuken and
 861 Silex) and in the two turbid-water ponds (Pêcheres and Leybeek). Other studies have found no difference in N₂O
 862 sedimentary production in lakes with high and low density of submerged macrophytes. We hypothesize that in human
 863 impacted system such as the urban ponds in the city of Brussels, the strong range of variations of DIN was the main driver of
 864 N₂O levels and over-rides other possible drivers such as presence or absence of macrophytes. Such a hypothesis was
 865 consistent with an overall positive relation between %N₂O and DIN in the urban ponds of the city of Brussels irrespective of
 866 presence or absence of macrophytes (Bauduin et al., 2024; this study). We hypothesize that CO₂ fluxes were relatively
 867 invariant among the four sampled ponds because of they were of similar size and depth, and that they were all relatively
 868 productive irrespective of whether from phytoplankton or submerged macrophytes.

The total (diffusive and ebullitive) CH₄ emissions represented 57.7±28.9 % (ranging seasonally from 4.9 to 99.9%) of total GHG emissions in CO₂-eq equivalents in the two clear-water ponds compared to 41.0±28.7 % (ranging seasonally from 2.8 to 99.9%) in the two turbid-water ponds. CO₂ represented nearly all the remainder of total GHG emissions in CO₂-eq, since and N₂O represented a very marginal fraction (0.8±1.6 %, ranging from 0.0% to 14.9%, with the maximum coinciding with minimal total CO₂-eq GHG flux in the Leybeek pond). The seasonal variations of GHG emissions were dominated by CH₄ ebullitive seasonal variations that peaked in summer (both quantitatively and relatively), as CH₄ ebullition was strongly related to temperature. The pCO₂ values in the four sampled ponds increased with precipitation at seasonal scale, probably in relation to higher inputs of organic and inorganic carbon by surface runoff. Years 2022 and 2023 were abnormally dry and wet, respectively, and consequently, ~~This seemed to have affected~~ the GHG emissions ~~that~~ were higher in 2023 mainly due to an increase in the relative contribution of CO₂ emissions, probably in response to a strong El Niño event. This would suggest that variations of precipitation also affected year-to-year variations of CO₂ emissions in addition to partly regulating seasonal variations of CO₂ emissions from the four studied ponds.

Data availability. ~~Full-Ti~~ timestamped and georeferenced data-set is available at 10.5281/zenodo.11103556.

Author contributions. AVB and NG conceived the study; TB collected field samples; TB and AVB made the laboratory analysis; TB and AVB jointly interpreted data and drafted the manuscript with substantial inputs from NG.

Competing interests. The authors declare that they have no conflict of interest.

Acknowledgements. We thank Ozan Efe (University of Liège) and Adriana Anzil (~~Free University of Brussels~~ Université Libre de Bruxelles) for analytical assistance, Florence Charlier (~~Free University of Brussels~~ Université Libre de Bruxelles) for help in macrophyte identification and density quantification (Table S1), Bruxelles Environnement for providing information on history of operations in the ponds (Table S2), and Cédric Morana (University of Liège) for help and advice in setting up the Picarro G2201-i isotopic analyzer, two anonymous reviewers for comments and suggestions on the initial manuscript. ~~AVB is a Research Director at the FRS-FNRS.~~

Financial support. TB received funding from the Brussels-Capital Region's institute for the encouragement of scientific research and innovation (Innoviris) as part of the Smartwater project (RBC/2020-EPF-6 h) and from the "Fonds pour la formation à la Recherche dans l'Industrie et dans l'Agriculture" (FRIA, Belgium). The Picarro G2201-i isotopic analyzer was funded by FRS-FNRS (U.N005.21). AVB is a Research Director at the FRS-FNRS.

References

- Aben, R. C. H., Barros, N., Van Donk, E., Frenken, T., Hilt, S., Kazanjian, G., Lamers, L. P. M., Peeters, E. T. H. M., Roelofs, J.G.M., de Senerpont Domis, L. S., Stephan, S., Velthuis, M., Van de Waal, D., Wik, M., Thornton, B., Wilkinson, J., Delsontro, T., and Kosten, S.: Cross continental increase in methane ebullition under climate change. *Nature communications*, 8(1), 1682. <https://doi.org/10.1038/s41467-017-01535-y>, 2017.
- Abril, G., Commarieu, M. V., and Guérin, F.: Enhanced methane oxidation in an estuarine turbidity maximum. *Limnology and oceanography*, 52(1), 470-475. <https://doi.org/10.4319/lo.2007.52.1.0470>, 2007.
- Audet, J., Carstensen, M.V., Hoffmann, C.C., Lavaux, L., Thieme, K., and Davidson, T.A.: Greenhouse gas emissions from urban ponds in Denmark. *Inland Waters* 10 (3), 373–385. <https://doi.org/10.1080/20442041.2020.1730680>, 2020.
- Baliña, S., Sanchez, M. L., Izaguirre, I., and del Giorgio, P. A.: Shallow lakes under alternative states differ in the dominant greenhouse gas emission pathways. *Limnology and Oceanography*, 68(1), 1-13. <https://doi.org/10.1002/lno.12243>, 2023.

- 906 Barko, J. W., Gunnison, D., and Carpenter, S. R.: Sediment interactions with submersed macrophyte growth and community dynamics.
907 *Aquatic botany*, 41(1-3), 41-65. [https://doi.org/10.1016/0304-3770\(91\)90038-7](https://doi.org/10.1016/0304-3770(91)90038-7), 1991.
- 908 Bartosiewicz, M., Maranger, R., Przytulska, A., and Laurion, I.: Effects of phytoplankton blooms on fluxes and emissions of greenhouse
909 gases in a eutrophic lake. *Water Research*, 196, 116985. <https://doi.org/10.1016/j.watres.2021.116985>, 2021.
- 910 Bastviken D., Ejlertsson J. and Tranvik L.: Measurement of methane oxidation in lakes: A comparison of methods. *Environmental*
911 *Science & Technology*, 36, 3354-3361. <https://doi.org/10.1021/es010311p>, 2002.
- 912 Bastviken, D., Cole, J. J., Pace, M. L., and Van de Bogert, M. C.: Fates of methane from different lake habitats: Connecting whole-lake
913 budgets and CH₄ emissions. *Journal of Geophysical Research: Biogeosciences*, 113(G2). <https://doi.org/10.1029/2007JG000608>, 2008.
- 914 Bastviken, D., Cole, J., Pace, M., and Tranvik, L.: Methane emissions from lakes: Dependence of lake characteristics, two regional
915 assessments, and a global estimate. *Global biogeochemical cycles*, 18(4). <https://doi.org/10.1029/2004GB002238>, 2004.
- 916 Bastviken, D., Treat, C.C., Pangala, S.R., Gauci, V., Enrich-Prast, A., Karlson, M., Gålfalk, M., Romano, M.B., and Sawakuchi, H.O.: The
917 importance of plants for methane emission at the ecosystem scale. *Aquat Bot* 184, 103596. <https://doi.org/10.1016/j.aquabot.2022.103596>,
918 2023.
- 919 Bauduin, T., Gypens, N., and Borges, A. V.: Seasonal and spatial variations of greenhouse gas (CO₂, CH₄ and N₂O) emissions from
920 urban ponds in Brussels. *Water Research*, 121257. <https://doi.org/10.1016/j.watres.2024.121257>, 2024.
- 921 Berberich, M. E., Beaulieu, J. J., Hamilton, T. L., Waldo, S., and Buffam, I.: Spatial variability of sediment methane production and
922 methanogen communities within a eutrophic reservoir: importance of organic matter source and quantity. *Limnol. Oceanogr.* 65, 1–23.
923 <https://doi.org/10.1002/lno.11392>, 2020.
- 924 Borges, A.V., Darchambeau, F., Lambert, T., Morana, C., Allen, G.H., Tambwe, E., and Bouillon, S.: Variations in dissolved greenhouse
925 gases (CO₂, CH₄, N₂O) in the Congo River network overwhelmingly driven by fluvial-wetland connectivity. *Biogeosciences* 16 (19),
926 3801–3834. <https://doi.org/10.5194/bg-16-3801-2019>, 2019.
- 927 Borges, A.V., Deirmendjian, L., Bouillon, S., Okello, W., Lambert, T., Roland, F.A.E., Razanamahandry, V.F., Voarintsoa, N.R.G.,
928 Darchambeau, F., Kimirei, I.A., Descy, J., Allen, G.H., and Morana, C.: Greenhouse gas emissions from African lakes are no longer a
929 blind spot. *Sci. Adv.* 8 (25), eabi8716. <https://doi.org/10.1126/sciadv.abi8716>, 2022.
- 930 Brans, K.I., Engelen, J.M., Souffreau, C., and De Meester, L.: Urban hot-tubs: local urbanization has profound effects on average and
931 extreme temperatures in ponds. *Landsc. Urban Plan.* 176, 22–29. <https://doi.org/10.1016/j.lup.2018.05.018>, 2018.
- 932 Cael, B. B., Heathcote, A. J., and Seekell, D. A.: The volume and mean depth of Earth's lakes. *Geophysical Research Letters*, 44(1), 209-
933 218. <https://doi.org/10.1002/2016GL071378>, 2017.
- 934 Casas-Ruiz, J.P., Jakobsson, J., and del Giorgio, P.A.: The role of lake morphometry in modulating surface water carbon concentrations in
935 boreal lakes. *Environ. Res. Lett.* 16 (7), 074037 <https://doi.org/10.1088/1748-9326/ac0be3>, 2021.
- 936 Chen, B., Zhang, L., and Wang, C.: Distinct impacts of the central and eastern Atlantic Niño on the European climate. *Geophysical*
937 *Research Letters*, 51(2), e2023GL107012. <https://doi.org/10.1029/2023GL107012>, 2024.
- 938 Choudhury, M. I., McKie, B. G., Hallin, S., and Ecke, F.: Mixtures of macrophyte growth forms promote nitrogen cycling in wetlands.
939 *Science of the Total Environment*, 635, 1436-1443. <https://doi.org/10.1016/j.scitotenv.2018.04.193>, 2018.
- 940 Clifford, C.C., and Heffernan, J.B.: Artificial aquatic ecosystems. *Water* 10 (8), 1096. <https://doi.org/10.3390/w10081096>, 2018.
- 941 Codispoti, L.A., and Christensen, J.P.: Nitrification, denitrification and nitrous oxide cycling in the eastern tropical South Pacific Ocean.
942 *Mar. Chem.* 16 (4), 277–300. [https://doi.org/10.1016/0304-4203\(85\)90051-9](https://doi.org/10.1016/0304-4203(85)90051-9), 1985.
- 943 Cole, J.J., and Caraco, N.F.: Atmospheric exchange of carbon dioxide in a low-wind oligotrophic lake measured by the addition of SF₆.
944 *Limnol. Oceanogr.* 43 (4), 647–656. <https://doi.org/10.4319/lo.1998.43.4.0647>, 2018.
- 945 Coleman, D. D., Risatti, J. B., and Schoell, M.: Fractionation of carbon and hydrogen isotopes by methane oxidizing bacteria. *Geochimica*
946 *Cosmochimica Acta*, 45, 1033–1037. [https://doi.org/10.1016/0016-7037\(81\)90129-0](https://doi.org/10.1016/0016-7037(81)90129-0), 1981.
- 947 Conrad, R., Noll, M., Claus, P., Klose, M., Bastos, W. R., and Enrich-Prast, A.: Stable carbon isotope discrimination and microbiology of
948 methane formation in tropical anoxic lake sediments. *Biogeosciences*, 8(3), 795-814. <https://doi.org/10.5194/bg-8-795-2011>, 2011.
- 949 Conrad, R.: Control of Methane Production in Terrestrial Ecosystems, In: Andreae, M.O. and Schimel, D.S., Ed., *Exchange of Trace Gases*
950 *between Terrestrial Ecosystems and the Atmosphere*, John Wiley, New York, 39-58, 1989.

951 Conrad, R.: Quantification of methanogenic pathways using stable carbon isotopic signatures: a review and a proposal. *Organic*
952 *geochemistry*, 36(5), 739-752. <https://doi.org/10.1016/j.orggeochem.2004.09.006>, 2005.

953 Dan, Z., Chuan, W., Qiaohong, Z., and Xingzhong, Y.: Sediments nitrogen cycling influenced by submerged macrophytes growing in
954 winter. *Water Science and Technology*, 83(7), 1728-1738. <https://doi.org/10.2166/wst.2021.081>, 2021.

955 Davidson, T.A., Audet, J., Svenning, J.C., Lauridsen, T.L., Søndergaard, M., Landkildehus, F., and Jeppesen, E.: Eutrophication effects on
956 greenhouse gas fluxes from shallow-lake mesocosms override those of climate warming. *Glob. Chang. Biol.* 21 (12), 4449–4463.
957 <https://doi.org/10.1111/gcb.13062>, 2015.

958 Deemer, B. R., and Holgerson, M. A.: Drivers of methane flux differ between lakes and reservoirs, complicating global upscaling efforts.
959 *Journal of Geophysical Research: Biogeosciences*, 126(4) <https://doi.org/10.1029/2019JG005600>, 2021.

960 DelSontro, T., Beaulieu, J. J., and Downing, J. A.: Greenhouse gas emissions from lakes and impoundments: Upscaling in the face of
961 global change. *Limnology and Oceanography Letters*, 3(3), 64-75. <https://doi.org/10.1002/lol2.10073>, 2018.

962 DelSontro, T., L. Boutet, A. St-Pierre, P.A. del Giorgio, and Y.T.: Prairie, Methane ebullition and diffusion from northern ponds and lakes
963 regulated by the interaction between temperature and system productivity, *Limnol. Oceanogr.* 61(S1), S62-S77
964 <https://doi.org/10.1002/lno.10335>, 2016.

965 DelSontro, T., Kunz, M. J., Kempter, T., Wüest, A., Wehrli, B., and Senn, D. B.: Spatial Heterogeneity of Methane Ebullition in a Large
966 Tropical Reservoir, *Environmental Science & Technology* 45 (23), 9866-9873, <https://doi.org/10.1021/es2005545>, 2011.

967 Deng, Hg., Zhang, J., Wu, Jj., Yao, X., and Yang, L.-W.: Biological denitrification in a macrophytic lake: implications for macrophytes-
968 dominated lake management in the north of China. *Environ Sci Pollut Res* 27, 42460–42471. <https://doi.org/10.1007/s11356-020-10230-3>
969 , 2020.

970 Desrosiers, K., DelSontro, T., and del Giorgio, P. A.: Disproportionate Contribution of Vegetated Habitats to the CH₄ and CO₂ Budgets of
971 a Boreal Lake. *Ecosystems*, 1-20. <https://doi.org/10.1007/s10021-021-00730-9>, 2022.

972 Downing, J. A.: Emerging global role of small lakes and ponds: little things mean a lot. *Limnetica*, 29(1), 0009-24.
973 <https://doi.org/10.23818/limn.29.02>, 2009.

974 Dickson, A.G.; Sabine, C.L. and Christian, J.R.: Guide to best practices for ocean CO₂ measurement. Sidney, British Columbia, North
975 Pacific Marine Science Organization, 191pp. (PICES Special Publication 3; IOCCP Report 8). <https://doi.org/10.25607/OBP-1342>, 2007.

976 Dumestre, J. F., Guézennec, J., Galy-Lacaux, C., Delmas, R., Richard, S., and Labroue, L.: Influence of light intensity on methanotrophic
977 bacterial activity in Petit Saut Reservoir, French Guiana. *Applied and environmental microbiology*, 65(2), 534-539.,
978 <https://doi.org/10.1128/aem.65.2.534-539.1999>, 1999.

979 Dutton, G., Elkins II, J., Hall, B., NOAA ESRL, Earth System Research Laboratory Halocarbons and Other Atmospheric Trace Gases
980 Chromatograph for Atmospheric Trace Species (CATS) Measurements. NOAA National Centers for Environmental Information.
981 <https://doi.org/10.7289/V5X0659V>. Version 1. [Database: atmospheric nitrous oxide N₂O] [2024-03–27], 2017.

982 Goeckner, A. H., Lusk, M. G., Reisinger, A. J., Hosen, J. D., and Smoak, J. M.: Florida's urban stormwater ponds are net sources of
983 carbon to the atmosphere despite increased carbon burial over time. *Communications earth & environment*, 3(1), 53,
984 <https://doi.org/10.1038/s43247-022-00384-y> 2022.

985 Gorsky, A.L., Racanelli, G.A., Belvin, A.C., and Chambers, R.M.: Greenhouse gas flux from stormwater ponds in southeastern Virginia
986 (USA). *Anthropocene* 28, 100218. <https://doi.org/10.1016/j.ancene.2019.100218>, 2019.

987 Gorsky, A. L., Dugan, H. A., Wilkinson, G. M., and Stanley, E. H.: Under-ice oxygen depletion and greenhouse gas supersaturation in
988 north temperate urban ponds. *Journal of Geophysical Research: Biogeosciences*, 129(6), <https://doi.org/10.1029/2024JG008120>, 2024.

989 Grasset, C., Abril, G., Mendonça, R., Roland, F., and Sobek, S.: The transformation of macrophyte-derived organic matter to methane
990 relates to plant water and nutrient contents. *Limnology and Oceanography*, 64(4), 1737-1749, <https://doi.org/10.1002/lno.11148>, 2019.

991 Grasset, C., Sobek, S., Scharnweber, K., Moras, S., Villwock, H., Andersson, S., Hiller, C., Nydahl, A.C., Chaguaceda, F., Colom, W., and
992 Tranvik, L.J.: The CO₂-equivalent balance of freshwater ecosystems is non-linearly related to productivity. *Glob. Chang. Biol.* 26 (10),
993 5705–5715. <https://doi.org/10.1111/gcb.15284>, 2020.

994 Grasshoff, K., and Johannsen, H.: A new sensitive and direct method for the automatic determination of ammonia in sea water. *ICES J.*
995 *Mar. Sci.* 34 (3), 516–521. <https://doi.org/10.1093/icesjms/34.3.516>, 1972.

- 996 Grasshoff, K., Kremling, K., and Ehrhardt, M.: Methods of Seawater Analysis: Determination of Nitrite. John Wiley & Sons, 2009.
- 997 Greinert J., and D.F. McGinnis: Single bubble dissolution model – The graphical user interface SiBu-GUI, Environmental Modelling &
998 Software, 24, 1012-1013, <https://doi.org/10.1016/j.envsoft.2008.12.011>, 2009.
- 999 Grinham, A., Albert, S., Deering, N., Dunbabin, M., Bastviken, D., Sherman, B., Lovelock, C.E., and Evans, C.D.: The importance of
1000 small artificial water bodies as sources of methane emissions in Queensland, Australia. Hydrol. Earth Syst. Sci. 22 (10), 5281–5298.
1001 <https://doi.org/10.5194/hess-22-5281-2018>, 2018.
- 1002 Harpenslager, S. F., Thiemer, K., Levertz, C., Misteli, B., Sebola, K. M., Schneider, S. C., Hilt, S., and Köhler, J.: Short-term effects of
1003 macrophyte removal on emission of CO₂ and CH₄ in shallow lakes. *Aquatic Botany*, 182, 103555.
1004 <https://doi.org/10.1016/j.aquabot.2022.103555>, 2022.
- 1005 Herrero Ortega, S., Romero Gonz´alez-Quijano, C., Casper, P., Singer, G.A., and Gessner, M.O.: Methane emissions from contrasting
1006 urban freshwaters: rates, drivers, and a whole-city footprint. Glob. Chang. Biol. 25 (12), 4234–4243. <https://doi.org/10.1111/gcb.14799>,
1007 2019.
- 1008 Hilt, S., Brothers, S., Jeppesen, E., Veraart, A. J., and Kosten, S.: Translating regime shifts in shallow lakes into changes in ecosystem
1009 functions and services. *BioScience*, 67(10), 928-936. <https://doi.org/10.1093/biosci/bix106>, 2017.
- 1010 Holgerson, M., and Raymond, P.: Large contribution to inland water CO₂ and CH₄ emissions from very small ponds. Nat. Geosci. 9, 222–
1011 226. <https://doi.org/10.1038/ngeo2654>, 2016.
- 1012 Holgerson, MA.: Drivers of carbon dioxide and methane supersaturation in small, temporary ponds, *Biogeochemistry* 124:305–318.
1013 <https://doi.org/10.1007/s10533-015-0099-y>, 2015.
- 1014 Huttunen, J. T., Alm, J., Liikanen, A., Juutinen, S., Larmola, T., Hammar, T., Silvola, T., and Martikainen, P. J.: Fluxes of methane,
1015 carbon dioxide and nitrous oxide in boreal lakes and potential anthropogenic effects on the aquatic greenhouse gas emissions.
1016 *Chemosphere*, 52(3), 609-621. [https://doi.org/10.1016/S0045-6535\(03\)00243-1](https://doi.org/10.1016/S0045-6535(03)00243-1), 2003.
- 1017 Hyvönen, T., Ojala, A., Kankaala, P., & Martikainen, P. J.: Methane release from stands of water horsetail (*Equisetum fluviatile*) in a
1018 boreal lake, *Freshwat. Biol.*, 40, 275– 284. <https://doi.org/10.1046/j.1365-2427.1998.00351.x>, 1998.
- 1019 Johnson, M.S., Matthews, E., Du, J., Genovese, V., and Bastviken, D.: Methane Emission from Global Lakes: New Spatiotemporal Data
1020 and Observation-Driven Modeling of Methane Dynamics Indicates Lower Emissions. *Journal of Geophysical Research: Biogeosciences*,
1021 127(7). <https://doi.org/10.1029/2022JG006793>, 2022.
- 1022 Juutinen, S., Alm, J., Larmola, T., Huttunen, J. T., Morero, M., Martikainen, P. J., and Silvola, J.: Major implication of the littoral zone for
1023 methane release from boreal lakes, *Global Biogeochem. Cycles*, 17(4), 1117, <https://doi.org/10.1029/2003GB002105>, 2003.
- 1024 Kankaala, P., Huotari, J., Peltomaa, E., Saloranta, T., and Ojala, A.: Methanotrophic activity in relation to methane efflux and total
1025 heterotrophic bacterial production in a stratified, humic, boreal lake. *Limnology and Oceanography*, 51(2), 1195-1204.
1026 <https://doi.org/10.4319/lo.2006.51.2.1195>, 2006.
- 1027 Kankaala, P., Huotari, J., Tulonen, T., & Ojala, A.: A Lake-size dependent physical forcing drives carbon dioxide and methane effluxes
1028 from lakes in a boreal landscape. *Limnol Oceanogr* 58:1915–1930. <https://doi.org/10.4319/lo.2013.58.6.1915>, 2013.
- 1029 Keller, M., and R. F. Stallard: Methane emission by bubbling from Gatun Lake, Panama, *J. Geophys. Res.*, 99(D4), 8307–8319,
1030 doi:[10.1029/92JD02170](https://doi.org/10.1029/92JD02170), 1994.
- 1031 Kelly, C. A., and Chynoweth, D. P.: The contributions of temperature and of the input of organic matter in controlling rates of sediment
1032 methanogenesis 1. *Limnology and Oceanography*, 26(5), 891-897. <https://doi.org/10.4319/lo.1981.26.5.0891>, 1981.
- 1033 Kirchman D., and Mitchell, R.: Contribution of Particle-Bound Bacteria to Total Microheterotrophic Activity in Five Ponds and Two
1034 Marshes, *Applied And Environmental Microbiology*, 43, 200-209, <https://doi.org/10.1128/aem.43.1.200-209.1982>, 1982.
- 1035 Koroleff, J.: Determination of total phosphorus by alkaline persulphate oxidation. *Methods of Seawater Analysis*. Verlag Chemie,
1036 Weinheim, pp. 136–138, 1983.
- 1037 Kotsyurbenko, O. R., Friedrich, M. W., Simankova, M. V., Nozhevnikova, A. N., Golyshin, P. N., Timmis, K. N., and Conrad, R.: Shift
1038 from acetoclastic to H₂-dependent methanogenesis in a West Siberian peat bog at low pH values and isolation of an acidophilic
1039 *Methanobacterium* strain. *Applied and Environmental Microbiology*, 73(7), 2344-2348. <https://doi.org/10.1128/AEM.02413-06>, 2007.
- 1040 Lan, X., K.W. Thoning, and E.J. Dlugokencky: Trends in globally-averaged CH₄, N₂O, and SF₆ determined from NOAA Global
1041 Monitoring Laboratory measurements [data set]. Version 2024-08, <https://doi.org/10.15138/P8XG-AA10>, 2024.

- 1043 Lauerwald, R., Regnier, P., Figueiredo, V., Enrich-Prast, A., Bastviken, D., Lehner, B., Maavara, T., and Raymond, P.: Natural Lakes Are
1044 a Minor Global Source of N₂O to the Atmosphere. *Global Biogeochemical Cycles*, 33(12), 1564–1581.
1045 <https://doi.org/10.1029/2019GB006261>, 2019.
- 1046 Lauerwald, R., Allen, G. H., Deemer, B. R., Liu, S., Maavara, T., Raymond, P., Alcott, L., Bastviken, D., Hastie, A., Holgerson, M.A.,
1047 Johnson, M. S., Lehner, B., Lin, P., Marzadri, A., Ran, L., Tian, H., Yang, X., Yao, Y., and Regnier, P.: Inland water greenhouse gas
1048 budgets for RECCAP2: 2. Regionalization and homogenization of estimates. *Global Biogeochemical Cycles*, 37,
1049 e2022GB007658. <https://doi.org/10.1029/2022GB007658>, 2023.
- 1050 Li, C., Hambright, K. D., Bowen, H. G., Trammell, M. A., Grossart, H. P., Burford, M. A., Hamilton, D.P., Jiang, H., Latour, D., Meyer,
1051 E. I., Padisák, J., Zamor, R. M. and Krumholz, L. R.: Global co-occurrence of methanogenic archaea and methanotrophic bacteria in
1052 Microcystis aggregates, *Environmental Microbiology*, 23(11)<https://doi.org/10.1111/1462-2920.15691>, 2021.
- 1053 Liptay, K., Chanton, J., Czepiel, P., and Mosher, B.: Use of stable isotopes to determine methane oxidation in landfill cover soils. *Journal*
1054 *of Geophysical Research: Atmospheres*, 103(D7), 8243–8250. <https://doi.org/10.1029/97JD02630>, 1998.
- 1055 Liu, Y., Conrad, R., Yao, T., Gleixner, G., and Claus, P.: Change of methane production pathway with sediment depth in a lake on the
1056 Tibetan plateau. *Palaeogeography, Palaeoclimatology, Palaeoecology*, 474, 279–286. <https://doi.org/10.1016/j.palaeo.2016.06.021>, 2017.
- 1057 Maavara, T., Lauerwald, R., Laruelle, G. G., Akbarzadeh, Z., Bouskill, N. J., Van Cappellen, P., and Regnier, P.: Nitrous oxide emissions
1058 from inland waters: Are IPCC estimates too high? *Global Change Biology*, 25(2), 473–488. <https://doi.org/10.1111/gcb.145042>, 2019.
- 1059 Marotta, H., Duarte, C. M., Pinho, L., and Enrich-Prast, A.: Rainfall leads to increased pCO₂ in Brazilian coastal lakes. *Biogeosciences*,
1060 7(5), 1607–1614. <https://doi.org/10.5194/bg-7-1607-2010>, 2010.
- 1061 Martinez-Cruz, K., Gonzalez-Valencia, R., Sepulveda-Jauregui, A., Plascencia- Hernandez, F., Belmonte-Izquierdo, Y., and Thalasso, F.:
1062 Methane emission from aquatic ecosystems of Mexico City. *Aquat. Sci.* 79, 159–169. <https://doi.org/10.1007/s00027-016-0487-y>, 2017.
- 1063 McCrackin, M.L., and Elser, J. J.: Atmospheric nitrogen deposition influences denitrification and nitrous oxide production in lakes,
1064 *Ecology*, 91(2):528–39. <https://doi.org/10.1890/08-2210.1>, 2010.
- 1065 McGinnis, D.F., Greinert, J., Artemov, Y., Beaubien, S.E., and Wüest, A.: The fate of rising methane bubbles in stratified waters: what
1066 fraction reaches the atmosphere? *Journal of Geophysical Research* 111, C09007. <https://doi.org/10.1029/2005JC003183>, 2006.
- 1067 Mengis, M., Gächter, R., and Wehrli, B.: Sources and sinks of nitrous oxide (N₂O) in deep lakes. *Biogeochemistry*, 38, 281–301.
1068 <https://doi.org/10.1023/A:1005814020322>, 1997.
- 1069 Morana, C., Bouillon, S., Nolla-Ardèvol, V., Roland, F. A., Okello, W., Descy, J. P., Nankabirwa, A., Nabafu, E., Springael, D., and
1070 Borges, A. V.: Methane paradox in tropical lakes? Sedimentary fluxes rather than pelagic production in oxic conditions sustain
1071 methanotrophy and emissions to the atmosphere, *Biogeosciences*, 17, 5209–5221, <https://doi.org/10.5194/bg-17-5209-2020>, 2020.
- 1072 Morana C., Borges A.V., Roland F.A.E., Darchambeau F., Descy J.-P. and Bouillon S.: Methanotrophy within the water column of a large
1073 meromictic tropical lake (Lake Kivu, East Africa). *Biogeosciences*, 12, 2077–2088. <https://doi.org/10.5194/bg-12-2077-2015>, 2015.
- 1074 Murase, J., and Sugimoto, A.: Inhibitory effect of light on methane oxidation in the pelagic water column of a mesotrophic lake (Lake
1075 Biwa, Japan). *Limnology and oceanography*, 50(4), 1339–1343. <https://doi.org/10.4319/lo.2005.50.4.1339>, 2005.
- 1076 Natchimuthu, S., Panneer Selvam, B., and Bastviken, D.: Influence of weather variables on methane and carbon dioxide flux from a
1077 shallow pond. *Biogeochemistry* 119, 403–413. <https://doi.org/10.1007/s10533-014-9976-z>, 2014.
- 1078 Ni, M., Liang, X., Hou, L., Li, W., and He, C.: Submerged macrophytes regulate diurnal nitrous oxide emissions from a shallow eutrophic
1079 lake: A case study of Lake Wuliangsu in the temperate arid region of China. *Science of The Total Environment*, 811, 152451.
1080 <https://doi.org/10.1016/j.scitotenv.2021.152451>, 2022a.
- 1081 Ni, R., Xu, C., Shi, X., Yang, S., Li, L., Peng, X., and Song, L.: Acetoclastic methanogenesis pathway stability despite the high microbial
1082 taxonomic variability in the transition from acidogenesis to methanogenesis during food waste anaerobic digestion. *Journal of Cleaner*
1083 *Production*, 372, 133758. <https://doi.org/10.1016/j.jclepro.2022.133758>, 2022b.
- 1084 Ollivier, Q.R., Maher, D.T., Pitfield, C., and Macreadie, P.I.: Punching above their weight: large release of greenhouse gases from small
1085 agricultural dams. *Glob. Chang. Biol.* 25 (2), 721–732. <https://doi.org/10.1111/gcb.14477>, 2019.
- 1086 Palacin-Lizarbe, C., Camarero, L., Hallin, S., Jones, C. M., and Catalan, J.: Denitrification rates in lake sediments of mountains affected by
1087 high atmospheric nitrogen deposition. *Sci Rep* 10, 3003. <https://doi.org/10.1038/s41598-020-59759-w>, 2020.

- 1088 Peacock, M., Audet, J., Bastviken, D., Cook, S., Evans, C.D., Grinham, A., Holgerson, M. A., Högbom, L., Pickard, A.E., Zieliński, P.,
1089 and Futter, M.N.: Small artificial waterbodies are widespread and persistent emitters of methane and carbon dioxide. *Glob. Chang. Biol.*
1090 27 (20), 5109–5123. <https://doi.org/10.1111/gcb.15762>, 2021.
- 1091 Peacock, M., Audet, J., Jordan, S., Smeds, J., and Wallin, M.B.: Greenhouse gas emissions from urban ponds are driven by nutrient status
1092 and hydrology. *Ecosphere* 10 (3), e02643. <https://doi.org/10.1002/ecs2.2643>, 2019.
- 1093 Peretyatko, A., Symoens, J. J., and Triest, L.: Impact of macrophytes on phytoplankton in eutrophic peri-urban ponds, implications for
1094 pond management and restoration. *Belgian Journal of Botany*, 83-99. <https://doi.org/10.2307/20794626>, 2007.
- 1095 Rabaey, J. and Cotner, J.: Pond greenhouse gas emissions controlled by duckweed coverage. *Front. Environ. Sci.* 10, 889289
1096 <https://doi.org/10.3389/fenvs.2022.889289>, 2022.
- 1097 Rabaey, J. S., and Cotner, J. B.: The influence of mixing on seasonal carbon dioxide and methane fluxes in ponds. *Biogeochemistry*, 1-18,
1098 <https://doi.org/10.1007/s10533-024-01167-7>, 2024.
- 1099 Ray, N. E., & Holgerson, M. A.: High Intra-Seasonal Variability in Greenhouse Gas Emissions from Temperate Constructed Ponds.
1100 *Geophysical Research Letters*, 50(18), e2023GL104235, <https://doi.org/10.1029/2023GL104235>, 2023
- 1101 Ray, N. E., Holgerson, M. A., Andersen, M. R., Bikše, J., Bortolotti, L. E., Futter, M., Kokorite, I., Law, A., McDonald, C., Mesman, J.P.,
1102 Peacock, M., Richardson, D.C., Arsenaault, J., Bansal, S., Cawley, K., Kuhn, M., Shahabinia, A.R., and Smuifer, F.: Spatial and temporal
1103 variability in summertime dissolved carbon dioxide and methane in temperate ponds and shallow lakes. *Limnology and Oceanography*,
1104 68(7), 1530-1545. <https://doi.org/10.1002/lno.12362>, 2023.
- 1105
- 1106 Raymond, P. A., Hartmann, J., Lauerwald, R., Sobek, S., McDonald, C., Hoover, M., Butman, D., Striegl, R., Mayorga, E., Humborg, C.,
1107 Kortelainen, P., Dürr, H., Meybeck, M., Ciais, P., and Guth, P.: Global carbon dioxide emissions from inland waters. *Nature*, 503(7476),
1108 355–359. <https://doi.org/10.1038/nature12760>, 2013.
- 1109 Reis, P.C.J., Thottathil, S.D. and Prairie, Y.T. The role of methanotrophy in the microbial carbon metabolism of temperate lakes. *Nat*
1110 *Commun* 13, 43. <https://doi.org/10.1038/s41467-021-27718-2>, 2022.
- 1111 Reitsema, R. E., Meire, P., and Schoelynck, J.: The future of freshwater macrophytes in a changing world: dissolved organic carbon
1112 quantity and quality and its interactions with macrophytes. *Frontiers in Plant Science*, 9, 301954. <https://doi.org/10.3389/fpls.2018.00629>,
1113 2018.
- 1114 Rocher-Ros, G., Stanley, E. H., Loken, L. C., Casson, N. J., Raymond, P. A., Liu, S., Amatulli, G., and Sponseller, R. A.: Global methane
1115 emissions from rivers and streams. *Nature* 621:530–535. <https://doi.org/10.1038/s41586-023-06344-6>, 2023.
- 1116 Rosentreter, J. A., Borges, A. V., Deemer, B. R., Holgerson, M. A., Liu, S., Song, C., Melack, J., Raymond, P. A., Duarte, C. M., Allen, G.
1117 H., Olefeldt, D., Poulter, B., Battin, T. I., and Eyre, B. D.: Half of global methane emissions come from highly variable aquatic ecosystem
1118 sources. *Nature Geoscience*, 14(4), 225–230. <https://doi.org/10.1038/s41561-021-00715-2>, 2021.
- 1119 Sand-Jensen, K., & Staehr, P. A.: Scaling of pelagic metabolism to size, trophy and forest cover in small Danish lakes. *Ecosystems*, 10,
1120 128-142. <https://doi.org/10.1007/s10021-006-9001-z>, 2007.
- 1121 Scandella, B. P., Varadharajan, C., Hemond, H. F., Ruppel, C., and Juanes, R.: A conduit dilation model of methane venting from lake
1122 sediments. *Geophysical Research Letters*, 38(6). <https://doi.org/10.1029/2011GL046768>, 2011.
- 1123 Scheffer, M., Hosper, S. H., Meijer, M. L., Moss, B., and Jeppesen, E. (1993). Alternative equilibria in shallow lakes. *Trends in ecology &*
1124 *evolution*, 8(8), 275-279. [https://doi.org/10.1016/0169-5347\(93\)90254-M](https://doi.org/10.1016/0169-5347(93)90254-M)
- 1125 Schulz S., Matsuyama, H., and Conrad, R.: Temperature dependence of methane production from different precursors in a profundal
1126 sediment (Lake Constance) *FEMS Microbiology Ecology*, 22, 207-213; <https://doi.org/10.1111/j.1574-6941.1997.tb00372.x>, 1997.
- 1127 Schulz S., and Conrad, R.: Influence of temperature on pathways to methane production in the permanently cold profundal sediment of
1128 Lake Constance. *FEMS Microbiology Ecology* 201- I4; <https://doi.org/10.1111/j.1574-6941.1996.tb00299.x>, 1996.
- 1129 Singh, S.N., Kulshreshtha, K., and Agnihotri, S.: Seasonal dynamics of methane emission from wetlands. *Chemosphere Glob. Chang. Sci.*
1130 2 (1), 39–46. [https://doi.org/10.1016/S1465-9972\(99\)00046-X](https://doi.org/10.1016/S1465-9972(99)00046-X), 2000.
- 1131 Stanley, E. H., Casson, N. J., Christel, S. T., Crawford, J. T., Loken, L. C., and Oliver, S. K.: The ecology of methane in streams and
1132 rivers: patterns, controls, and global significance. *Ecological Monographs*, 86(2), 146–171. <https://doi.org/10.1890/15-1027>, 2016.

- 1133 Taoka, T., Iwata, H., Hirata, R., Takahashi, Y., Miyabara, Y., and Itoh, M.: Environmental controls of diffusive and ebullitive methane
1134 emissions at a subdaily time scale in the littoral zone of a midlatitude shallow lake. *Journal of Geophysical Research: Biogeosciences*, 125,
1135 e2020JG005753. <https://doi.org/10.1029/2020JG005753>, 2020.
- 1136 Theus, M. E., Ray, N. E., Bansal, S., and Holgerson, M. A.: Submersed macrophyte density regulates aquatic greenhouse gas emissions.
1137 *Journal of Geophysical Research: Biogeosciences*, 128(10), <https://doi.org/10.1029/2023JG007758>, 2023.
- 1138 Tokida, T., Miyazaki, T., Mizoguchi, M., Nagata, O., Takakai, F., Kagemoto, A., and Hatano, R.: Falling atmospheric pressure as a trigger
1139 for methane ebullition from peatland. *Global Biogeochemical Cycles*, 21(2). <https://doi.org/10.1029/2006GB002790>, 2007.
- 1140 Vachon, D., Langenegger, T., Donis, D., Beaubien, S. E., and McGinnis, D. F.: Methane emission offsets carbon dioxide uptake in a small
1141 productive lake. *Limnology and Oceanography Letters*, 5(6), 384-392, <https://doi.org/10.1002/lol2.10161>, 2020.
- 1142 van Bergen, T.J.H.M., Barros, N., Mendonça, R., Aben, R.C.H., Althuizen, I.H.J., Huszar, V., Lamers, L.P.M., Lüring, M., Roland, F.,
1143 and Kosten, S.: Seasonal and diel variation in greenhouse gas emissions from an urban pond and its major drivers. *Limnol. Oceanogr.* 64
1144 (5), 2129–2139. <https://doi.org/10.1002/lno.11173>, 2019.
- 1145 Varadharajan, C., and Hemond, H. F.: Time-series analysis of high-resolution ebullition fluxes from a stratified, freshwater lake. *Journal*
1146 *of Geophysical Research: Biogeosciences*, 117(G2). <https://doi.org/10.1029/2011JG001866>, 2012.
- 1147 Verpoorter, C., Kutser, T., Seekell, D. A., and Tranvik, L. J.: A global inventory of lakes based on high-resolution satellite imagery.
1148 *Geophysical Research Letters*, 41(18), 6396-6402. <https://doi.org/10.1002/2014GL060641>, 2014.
- 1149 Wang, T., Zhumabieke, M., Zhang, N., Liu, C., Zhong, J., Liao, Q., and Zhang, L.: Variable promotion of algae and macrophyte organic
1150 matter on methanogenesis in anaerobic lake sediment. *Environmental Research*, 237, 116922.
1151 <https://doi.org/10.1016/j.envres.2023.116922>, 2023.
- 1152 Wang, Z., Wang, S., Hu, Y., Du, B., Meng, J., Wu, G., Liu, H., and Zhan, X.: Distinguishing responses of acetoclastic and
1153 hydrogenotrophic methanogens to ammonia stress in mesophilic mixed cultures. *Water Research*, 224, 119029.
1154 <https://doi.org/10.1016/j.watres.2022.119029>, 2022.
- 1155 Wanninkhof, R.: Relationship between gas exchange and wind speed over the ocean. *J. Geophys. Res.* 97, 7373–7381.
1156 <https://doi.org/10.1029/92JC00188>, 1992.
- 1157 Webb, J.R., Leavitt, P.R., Simpson, G.L., Baulch, H.M., Haig, H.A., Hodder, K.R., and Finlay, K.: Regulation of carbon dioxide and
1158 methane in small agricultural reservoirs: optimizing potential for greenhouse gas uptake. *Biogeosciences* 16 (21), 4211–4227.
1159 <https://doi.org/10.5194/bg-16-4211-2019>, 2019.
- 1160 Weiss, R. F., Price, B. A.: Nitrous oxide solubility in water and seawater. *Marine chemistry*, 8(4), 347-359., [doi.org/10.1016/0304-](https://doi.org/10.1016/0304-4203(80)90024-9)
1161 [4203\(80\)90024-9](https://doi.org/10.1016/0304-4203(80)90024-9), 1980.
- 1162 Weiss, R. F.: Determinations of carbon dioxide and methane by dual catalyst flame ionization chromatography and nitrous oxide by
1163 electron capture chromatography. *J. Chromatogr. Sci.* 19, 611–616. <https://doi.org/10.1093/chromsci/19.12.611>, 1981.
- 1164 West, W. E., Coloso, J. J., and Jones, S. E.: Effects of algal and terrestrial carbon on methane production rates and methanogen community
1165 structure in a temperate lake sediment. *Freshw. Biol.* 57, 949–955. <https://doi.org/10.1111/j.1365-2427.2012.02755.x>, 2012.
- 1166 Whiticar, M. J., Faber, E., and Schoell, M.: Biogenic methane formation in marine and freshwater environments: CO₂ reduction vs. acetate
1167 fermentation—isotope evidence. *Geochimica et Cosmochimica Acta*, 50(5), 693-709. [https://doi.org/10.1016/0016-7037\(86\)90346-7](https://doi.org/10.1016/0016-7037(86)90346-7), 1986.
- 1168 Wik, M., Crill, P. M., Varner, R. K., and Bastviken, D.: Multiyear measurements of ebullitive methane flux from three subarctic lakes. *J.*
1169 *Geophys. Res. Biogeosciences* 118:791 1307–1321. <https://doi.org/10.1002/jgrg.20103>, 2013.
- 1170 Wik, M., Thornton, B. F., Bastviken, D., MacIntyre, S., Varner, R. K., and Crill, P. M.: Energy input is primary controller of methane
1171 bubbling in subarctic lakes. *Geophysical Research Letters*, 41(2), 555-560. <https://doi.org/10.1002/2013GL058510>, 2014.
- 1172 Xun, F., Feng, M., Ma, S., Chen, H., Zhang, W., Mao, Z., Zhou, Y., Xiao, Q., Wu, Q. L., and Xing, P.: Methane ebullition fluxes and
1173 temperature sensitivity in a shallow lake. *Science of The Total Environment*, 912, 169589. <https://doi.org/10.1016/j.scitotenv.2023.169589>,
1174 2024.
- 1175 Yan, X., Xu, X., Ji, M., Zhang, Z., Wang, M., Wu, S., Wang, G., Zhang, C., and Liu, H.: Cyanobacteria blooms: A neglected facilitator of
1176 CH₄ production in eutrophic lakes. *Science of the total environment*, 651, 466-474. <https://doi.org/10.1016/j.scitotenv.2018.09.197>, 2019.

- 1177 Yang, Z., Zhao, Y., and Xia, X.: Nitrous oxide emissions from *Phragmites australis*-dominated zones in a shallow lake. *Environmental*
1178 *pollution*, 166, 116-124. <https://doi.org/10.1016/j.envpol.2012.03.006>, 2012.
- 1179 Yentsch, C.S., and Menzel, D.W.: A method for the determination of phytoplankton chlorophyll and phaeophytin by fluorescence. In:
1180 Deep Sea Research and Oceanographic Abstracts, 10. Elsevier, pp. 221–231. [https://doi.org/10.1016/0011-7471\(63\)90358-9](https://doi.org/10.1016/0011-7471(63)90358-9), 1963.
- 1181 Zhao, K., Tedford, E. W., Zare, M., and Lawrence, G. A.: Impact of atmospheric pressure variations on methane ebullition and lake
1182 turbidity during ice-cover. *Limnology and Oceanography Letters*, 6(5), 253-261. <https://doi.org/10.1002/lol2.10201>, 2021.